Conserved Ankyrin Repeat Proteins and Their NIMA Kinase Partners Regulate Extracellular Matrix Remodeling and Intracellular Trafficking in *Caenorhabditis elegans*

Vladimir Lažetić and David S. Fay[1]
Department of Molecular Biology, College of Agriculture and Natural Resources, University of Wyoming, Laramie, Wyoming 82071

ABSTRACT Molting is an essential developmental process in nematodes during which the epidermal apical extracellular matrix, the cuticle, is remodeled to accommodate further growth. Using genetic approaches, we identified a requirement for three conserved ankyrin repeat-rich proteins, MLT-2/ANKS6, MLT-3/ANKS3, and MLT-4/INVS, in *Caenorhabditis elegans* molting. Loss of *mlt* function resulted in severe defects in the ability of larvae to shed old cuticle and led to developmental arrest. Genetic analyses demonstrated that MLT proteins functionally cooperate with the conserved NIMA kinase family members NEKL-2/NEK8 and NEKL-3/NEK6/NEK7 to promote cuticle shedding. MLT and NEKL proteins were specifically required within the hyp7 epidermal syncytium, and fluorescently tagged *mlt* and *nekl* alleles were expressed in puncta within this tissue. Expression studies further showed that NEKL-2–MLT-2–MLT-4 and NEKL-3–MLT-3 colocalize within largely distinct assemblies of apical foci. MLT-2 and MLT-4 were required for the normal accumulation of NEKL-2 at the hyp7–seam cell boundary, and loss of *mlt-2* caused abnormal nuclear accumulation of NEKL-2. Correspondingly, MLT-3, which bound directly to NEKL-3, prevented NEKL-3 nuclear localization, supporting the model that MLT proteins may serve as molecular scaffolds for NEKL kinases. Our studies additionally showed that the NEKL–MLT network regulates early steps in clathrin-mediated endocytosis at the apical surface of hyp7, which may in part account for molting defects observed in *nekl* and *mlt* mutants. This study has thus identified a conserved NEKL–MLT protein network that regulates remodeling of the apical extracellular matrix and intracellular trafficking, functions that may be conserved across species.

KEYWORDS *C. elegans*; molting; NIMA kinase; endocytosis; ankyrin repeat proteins

MOLTING is a ubiquitous process in nematode species, including *Caenorhabditis elegans*, and is required for organismal growth and development. Although the observable biomechanics and major morphological features of *C. elegans* molting were first described nearly 40 years ago (Hirsh *et al.* 1976; Singh and Sulston 1978), the molecular and cellular mechanisms underlying this complex process are largely unknown. Notably, molting occurs in both pathogenic and nonpathogenic nematode species, and molting factors have been proposed as potential targets for antiparasitic drugs (Page *et al.* 2014; Gooyit *et al.* 2015).

Mechanistically, molting is the process by which nematodes remodel their epidermal apical extracellular matrix (ECM), termed the cuticle. In *C. elegans* larvae and adults, the cuticle serves as a mechanical barrier and provides physical and chemical protection from the environment (Page and Johnstone 2007). In addition, similar to the chitin-based exoskeleton of insects and other arthropods, the cuticle is required to facilitate organismal movement in conjunction with attached underlying muscles. Unlike arthropods, however, in nematodes the cuticle is comprised primarily of collagens (Page and Johnstone 2007) and thus may serve as a more proximate model for mammalian skin or for the ECM associated with mammalian tissues and organs. In mammals, ECM remodeling is essential for development, homoeostasis, and physiological wound healing (Cox and Erler 2011).

doi: 10.1534/genetics.116.194464
Manuscript received August 2, 2016; accepted for publication October 28, 2016; published Early Online October 31, 2016.
Supplemental material is available online at http://www.genetics.org/cgi/content/full/genetics.116.194464/DC1.
[1]Corresponding author: Department 3944, 1000 E. University Ave., Department of Molecular Biology, College of Agriculture and Natural Resources, University of Wyoming, Laramie, WY 82071. E-mail: davidfay@uwyo.edu

Deregulation of ECM remodeling has also been linked to a number of disease states, most notably cancer cell growth and metastasis (Cox and Erler 2011; Yu *et al.* 2011). Furthermore, the inappropriate deposition of collagens can lead to severe fibrotic diseases such as pulmonary fibrosis (Raghu *et al.* 1989; Specks *et al.* 1995; Todd *et al.* 2012), liver cirrhosis (Murata *et al.* 1984; Nielsen *et al.* 2014), cardiovascular diseases (Zannad and Radauceanu 2005), and systemic sclerosis (Ponticos *et al.* 2015). *C. elegans* molting thus represents a powerful genetic system for studying conserved molecular mechanisms controlling ECM remodeling.

The C. *elegans* molting process has been traditionally separated into two stages termed lethargus (including apolysis and synthesis) and ecdysis (Singh and Sulston 1978; Page and Johnstone 2007; Chisholm and Xu 2012). Initially, the animal gradually decreases physical activity and feeding and becomes lethargic. During apolysis, the larva partially detaches its old cuticle, which then allows for the synthesis of an underlying new cuticle by the epidermis. During ecdysis, a series of stereotypical movements lead to the complete detachment of the old cuticle, followed by the resumption of normal feeding and activities (Singh and Sulston 1978; Page and Johnstone 2007; Chisholm and Xu 2012). The rapid and precise regulation of these steps, which includes the attachment of body wall muscles to the newly synthesized cuticle, is essential to minimize vulnerability and maximize growth potential.

Forward genetics and RNA interference (RNAi) screens have identified a variety of genes that promote molting in *C. elegans* (Frand *et al.* 2005). Positive regulators of molting include matrix metalloproteases (Davis *et al.* 2004; Hashmi *et al.* 2004; Suzuki *et al.* 2004; Altincicek *et al.* 2010; Kim *et al.* 2011; Stepek *et al.* 2011), which are important for digestion of the old cuticle or processing of the new cuticle precursors, as well as selenoproteins, which promote collagen cross-linking (Stenvall *et al.* 2011). Other functional classes of molecules critical for molting include sterol-binding nuclear hormone receptors (NHRs) (Kostrouchova *et al.* 1998, 2001; Gissendanner and Sluder 2000; Hayes *et al.* 2006; Monsalve and Frand 2012), enzymes controlling sterol and fatty acid synthesis (Jia *et al.* 2002; Kuervers *et al.* 2003; Entchev and Kurzchalia 2005; Li and Paik 2011), and hedgehog-related proteins (Zugasti *et al.* 2005; Hao *et al.* 2006), which are often modified by sterols (Wendler *et al.* 2006) and are dependent on NHRs for expression (Kouns *et al.* 2011). Accordingly, dietary cholesterol promotes normal molting (Yochem *et al.* 1999; Merris *et al.* 2003; Entchev and Kurzchalia 2005; Roudier *et al.* 2005), along with the LRP-1/megalin lipoprotein receptor, which is thought to support lipid uptake by the epidermis (Yochem *et al.* 1999; May *et al.* 2007). Although these and other identified molting factors have provided insights into the general processes involved in *C. elegans* molting, the specific molecular and cellular mechanisms that underlie molting remain poorly understood.

We recently described functions for two highly conserved members of the NIMA kinase family, NEKL-2 and NEKL-3, in *C. elegans* molting (Yochem *et al.* 2015). NEKL-2 is orthologous to mammalian NEK8, which has been implicated in ciliogenesis (Mahjoub *et al.* 2005; Quarmby and Mahjoub 2005; Otto *et al.* 2008; Shiba *et al.* 2010; Zalli *et al.* 2012). Correspondingly, mutations in *NEK8* can lead to organogenesis defects resulting from ciliopathies (Mahjoub *et al.* 2005; Otto *et al.* 2008, 2011; Trapp *et al.* 2008; McCooke *et al.* 2012; Halbritter *et al.* 2013; Hoff *et al.* 2013; Manning *et al.* 2013; Delestre *et al.* 2015). NEKL-3 is the *C. elegans* ortholog of mammalian paralogs NEK6 and NEK7, which have been reported to control several processes associated with cell division and are linked to human cancer. Interestingly, our previous studies strongly implicate NEKL-2/NEK8 and NEKL-3/NEK6/NEK7 in cellular processes that are distinct from ciliogenesis and cell division and further implicate NEKL-2/NEK8 in the regulation of intracellular trafficking.

In this study, we have extended the NEKL protein network to include the conserved ankyrin repeat proteins MLT-2/ANKS6, MLT-3/ANKS3, and MLT-4/INVS. Our data suggest that this conserved NEKL–MLT network can be approximately divided into two functional units comprised of NEKL-2–MLT-2–MLT-4 and NEKL-3–MLT-3. Furthermore, we have shown that MLT proteins regulate the subcellular localization of NEKL kinases within the epidermis and may act as molecular scaffolds. Finally, we demonstrated that the NEKL–MLT protein network affects early steps in clathrin-mediated endocytosis in the epidermis. Our studies implicate conserved NIMA kinase family members and their ankyrin repeat partners in the regulation of fundamental cellular functions that have been previously overlooked.

Materials and Methods

Strains and maintenance

C. elegans strains were maintained according to standard protocols (Stiernagle 2006) and were propagated at 21°. Strains used in this study include N2/Bristol (wild type), LH374 [*mlt-4(tm1484)*; *mnEx173* (ZC15; pTG96)], RT1378 [*pwIs528(gfp::chc-1)*], SP2734 [*mlt-4(sv9) V*; *mnEx173* (*mlt-4(+)*; pTG96)], VC20044 [*nekl-3(gk296269[E282K])*], VC20136 [*nekl-3(gk296270[P224L])*], VC20396 [*nekl-2(gk323150[S351N])*], VC20590 [*nekl-2(gk113450[A85T])*], VC30086 [*nekl-2(gk412380[G279E])*], VC40715 [*nekl-3(gk774978[G118S])*], VC40946 [*nekl-3(gk894345[D228N])*], WY1098 [*mlt-3(fd72)*; *fdEx267* (WRM0610dD02; pTG96)], WY1117 [*mlt-2(fd71)*;*fdEx272* (WRM0610dG01; WRM0618cD05; WRM0620bC01; WRM0636cH02; WRM0633bB08; pTG96)], WY1114 [*nekl-2(fd88[P283A,P284S,P285T])*], WY1120 [*nekl-2(fd79[Y84L,G87H,G88H])*; *fdEx273* (pDF166; pTG96)], WY1122 [*nekl-2(fd81[Y84L,G88A])*], WY1129 [*nekl-2(fd83[Y84L,G88Q])*], WY1130 [*nekl-2(fd84[G87H, G88A,R92L])*; *fdEx278* (pDF166; pTG96)], WY1141 [*nekl-3(gk894345)* 3×-outcross], *WY1145 [nekl-2(fd81)*; *nekl-3(gk894345)*;*fdEx286(pDF153[nekl-3(+)]; pTG96)]*;*fdEx286* (pDF153*(nekl-3(+)*; pTG96)], WY1152 [*nekl-2(fd89[Y84L,*

G87A,G88Q]); *fdEx278* (pDF166; pTG96)], *WY1155 [nekl-2(fd90[Y84L,G87A,G88A])*; *fdEx278]*, WY1165 [*nekl-2(fd91[Y84L,G87A]*; *fdEx278)*], WY1169 [*mlt-2(fd95[mlt-2*::*mKate2*::*3xFlag])*], WY1174 [*nekl-2(fd100[nekl-2*::*NeonGreen*::*3×Flag])*], WY1180 [*nekl-3(fd106[nekl-3*::*mKate2*::*3×Flag])*], WY1183 [*mlt-3(fd109[mlt-3*::*mKate2*::*3×Flag])*], WY1191 [*mlt-4(fd114[mlt-4*::*gfp*::*3×Flag])*], WY1193 [*nekl-2(fd100[nekl-2*::*NeonGreen*::*3×Flag])*; *nekl-3(fd106[nekl-3*::*mKate2*::*3×Flag])*], WY1194 [*nekl-2(fd100[nekl-2*::*NeonGreen*::*3×Flag])*; *mlt-3(fd109[mlt-3*::*mKate2*::*3×Flag])*], WY1195 [*nekl-3(fd106[nekl-3*::*mKate2*::*3×Flag])*; *mlt-4(fd114[mlt-4*::*gfp*::*3×Flag])*], WY1196 [*mlt-2(fd95[mlt-2*::*mKate2*::*3×Flag])*; *mlt-4(fd114[mlt-4*::*gfp*::*3×Flag])*], WY1230 [*nekl-3(fd118[nekl-3*::*NeonGreen*::*3×Flag])*], WY1237 [*mlt-3(fd109[mlt-3*::*mKate2*::*3×Flag])*; *mlt-4(fd114[mlt-4*::*gfp*::*3×Flag])*], WY1238 [*mlt-3(fd109[mlt-3*::*mKate2*::*3×Flag])*; *nekl-3(fd118[nekl-3*::*NeonGreen*::*3×Flag])*], WY1239 [*nekl-2(fd100[nekl-2*::*NeonGreen*::*3×Flag])*; *mlt-4(sv9) V*; *mnEx173(zc15[mlt-4(+)]*; *pTG96)*], WY1241 [*nekl-3(fd118[nekl-3*::*NeonGreen*::*3×Flag])*; *mlt-4(sv9) V*; *mnEx173* (*mlt-4(+)*; pTG96)], WY1242 [*nekl-2(fd81)*; *nekl-3(gk894345)*; *pwIs528* (*gfp*::*chc-1*); *fdEx256*], WY1251 [*nekl-3(gk894345)*; *pwIs528*], and WY1253 [*nekl-2(fd81)*; *pwIs528*], WY1303 [*nekl-2(gk839)*; *fdEx256* (WRM0639aE11; WRM0636aD02; *sur-5*::*rfp*); *nekl-3(gk506)*; *mnEx174* (*F19H6*; pTG96)], WY1305 [*mlt-2(fd71)*; *fdEx309*; *mlt-3(fd72)*; *fdEx267*], WY1306 [*mlt-2(fd71)*; *fdEx309*; *mlt-4(tm1484)*; *mnEx173*] .

Isolation, mapping, and rescue of mlt-4 (sv9)

mlt-4(sv9) was identified in a screen for recessive mutations that affect the completion of molting. N2 P_0 worms were treated with 50 mM ethyl methanesulfonate (Brenner 1974), and F_1 progeny were placed three per plate on OP50 plates. After growth at 25°, plates were examined for the presence of F_2 progeny exhibiting defects in molting, including a failure to completely shed old cuticle. Because mutants exhibiting defective molting are often incapable of reaching adulthood, nonmutant siblings were individually isolated from candidate plates and strains were initially maintained as heterozygotes. Because none of the mutations proved to be temperature sensitive, a temperature of 20–22° was used for their maintenance and analysis.

sv9 was assigned to the right arm of LG V by means of bulk sequence analysis (Wicks *et al.* 2001) of single-nucleotide polymorphisms (SNPs) between the N2 strain and the Hawaiian strain CB4856. Mapping placed *mlt-4* between *unc-51* and *rol-9*; 21 cross-overs were observed between *unc-51* and *mlt-4*, and one was observed between *mlt-4* and *rol-9*. Viable Unc recombinants from a strain having the genotype *unc-51 mlt-4*/CB4856 were examined for the segregation of SNPs that could be digested by a restriction enzyme. Likewise, viable Roll recombinants were examined from a strain with the genotype *mlt-4 rol-9*/CB4856. Rescue of *sv9* was initially obtained with the complete ZC15 cosmid. Rescue of *sv9* not observed with individual injections of two overlapping PCR fragments, neither of which contained a complete ZC15.7 gene. In contrast, co-injection of these fragments resulted in robust rescue; homologous recombination within the overlapping region will create an intact ZC15.7 gene.

mRNA analysis

Total RNA was isolated from mixed-staged populations of N2 worms by means of TRIzol (Invitrogen, San Diego, CA). The 5′ end of *mlt-4* was determined using FirstChoice RNA ligase-mediated rapid amplification of cDNA (RLM-RACE) kit (Ambion, Austin, TX). The 3′ ends were determined by means of reagents supplied with the kit. For both ends, gene-specific primers were used in combination with primers provided with the kit. Internal splice sites were verified by RT-PCR by means of a cMaster RTplusPCR System kit (Eppendorf, Westbury, NY) and gene-specific primers.

Bioinformatics tools

Protein motif and domain predictions were obtained using http://smart.embl-heidelberg.de (Letunic *et al.* 2015) and elm.eu.org (Dinkel *et al.* 2016) (Figure 1 and Figure 2 and data not shown). Sequence alignments were created using ClustalW in the Biology Workbench (http://workbench.sdsc.edu/; San Diego Supercomputer Center) (Supplemental Material, Figure S1), in the Jalview program using Muscle (Figure S3, A and B), and with Clustal sequence alignment services (Figure S3C) (Waterhouse *et al.* 2009). The phylogenetic tree was created by aligning amino acid sequences of selected proteins using http://www.ebi.ac.uk/Tools/msa/mafft/ (Katoh and Standley 2013; McWilliam *et al.* 2013; Li *et al.* 2015). Alignment was subsequently reformatted in http://www.ebi.ac.uk/Tools/sfc/emboss_seqret/ (Rice *et al.* 2000), and the tree was built using http://darwin.uvigo.es/software/prottest2_server.html (Abascal *et al.* 2005) and http://itol.embl.de/upload.cgi (Letunic and Bork 2016) (Figure S2). Frequency plot sequence logos were created using WebLogo (http://weblogo.berkeley.edu/logo.cgi) (Crooks *et al.* 2004) (Figure S3). Protein 3D structure predictions were created using I-TASSER (http://zhanglab.ccmb.med.umich.edu/I-TASSER) (Zhang 2008; Roy *et al.* 2010; Yang *et al.* 2015). For mutant versions of NEKL-2, the wild-type prediction was assigned as a template to guide I-TASSER modeling (Figure S4). Visualization, interatomic contacts, and surface analyses of predicted three-dimensional models were carried out using UCSF Chimera 1.11 (Pettersen *et al.* 2004) (Figure S4). Raytraced images were produced using POV-Ray (retrieved from http://www.povray.org/download/; Persistence of Vision Pty.) (Figure S4). Venn diagrams were created using Venny (http://bioinfogp.cnb.csic.es/tools/venny), created by J. C. Oliveros (Figure S4A).

Microscopy and measurements

Fluorescent images were acquired using an Olympus IX81 inverted microscope with a spinning-disc confocal head (CSU-X1 Yokogawa). Confocal illumination was provided by an

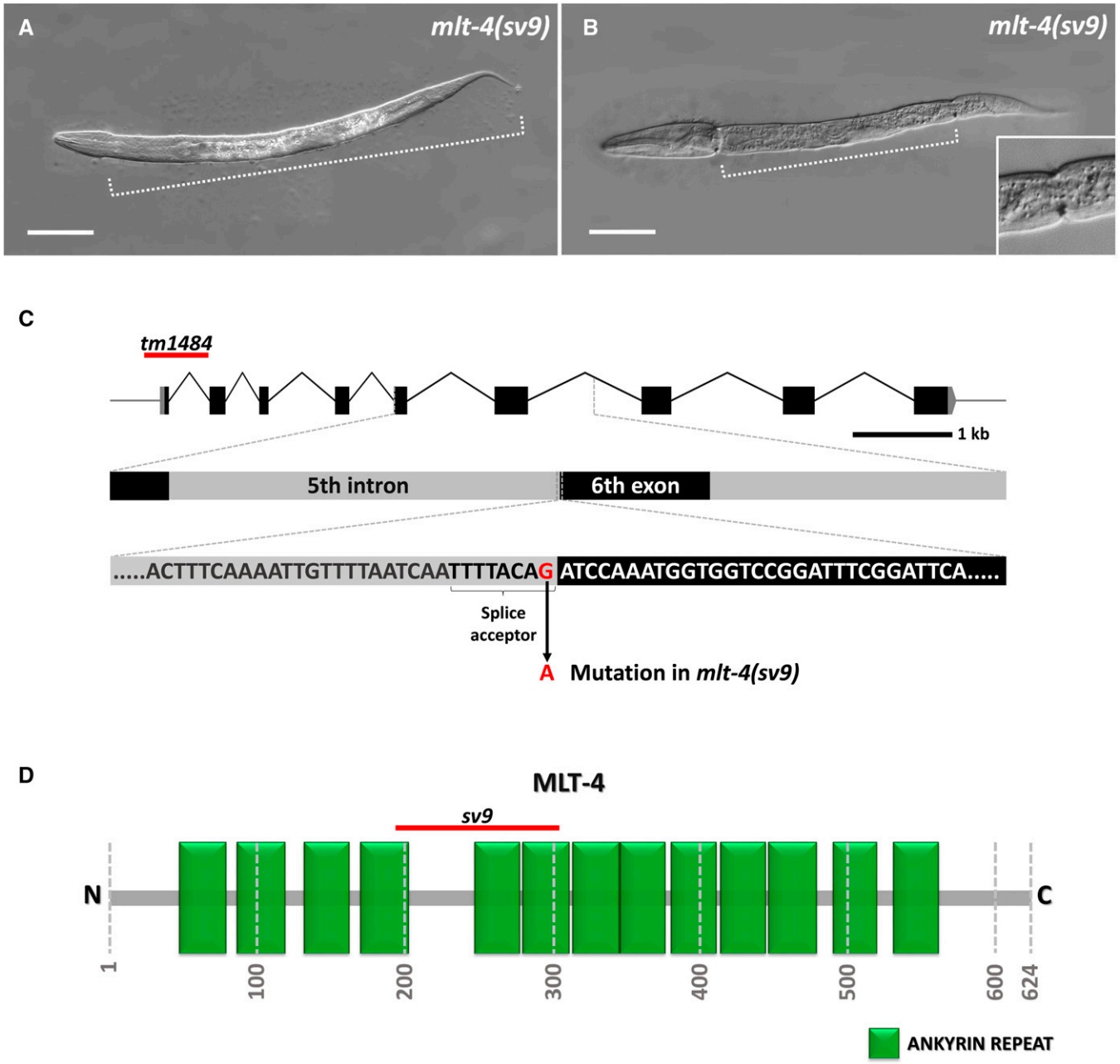

Figure 1 Molting defects in *mlt-4(sv9)* mutant animals. (A, B) DIC images of *sv9* homozygous larvae entrapped within two layers of cuticle. Dotted line indicates the extent of the constricted region containing both the old and new cuticle layers. A larva in which only the head region is free of old cuticle is shown in (A), whereas the larva in (B) displays a classic corset phenotype in which both the head and tail regions have released the old cuticle. The inset in (B) shows an enlargement of the posterior constriction. (C) Schematic representation of the *mlt-4 gene*; the affected region with the splice acceptor site that is mutated in the *sv9* allele is enlarged. The red line marks the location of the *tm1484* deletion. (D) Schematic illustration of MLT-4 with annotated predicted ankyrin repeats (green boxes). The red line indicates the region that would be affected by mis-splicing in *sv9* mutants. Numbers specify positions of amino acids. Bar, 50 μm (A, B).

ILE-4 laser launch (Spectral Applied Research). MetaMorph 7.7 software was used for image acquisition. During colocalization analyses, image registration of micrographs taken with different laser settings was performed with the Register Virtual Stack plugin in FIJI software. Registered images were merged, analyzed, and adjusted in ImageJ program. DIC images were acquired using a Nikon Eclipse epifluorescence microscope and Open Lab software. The same setup was used for measuring body length and width. Body width was measured in the central region of an animal, next to the vulva; 50 animals were scored for each category. Puncta movements were tracked and analyzed using MTrackJ plugin in ImageJ software. Animals were immobilized using a 0.1 M solution of levamisole. Nuclear staining was performed using Hoechst

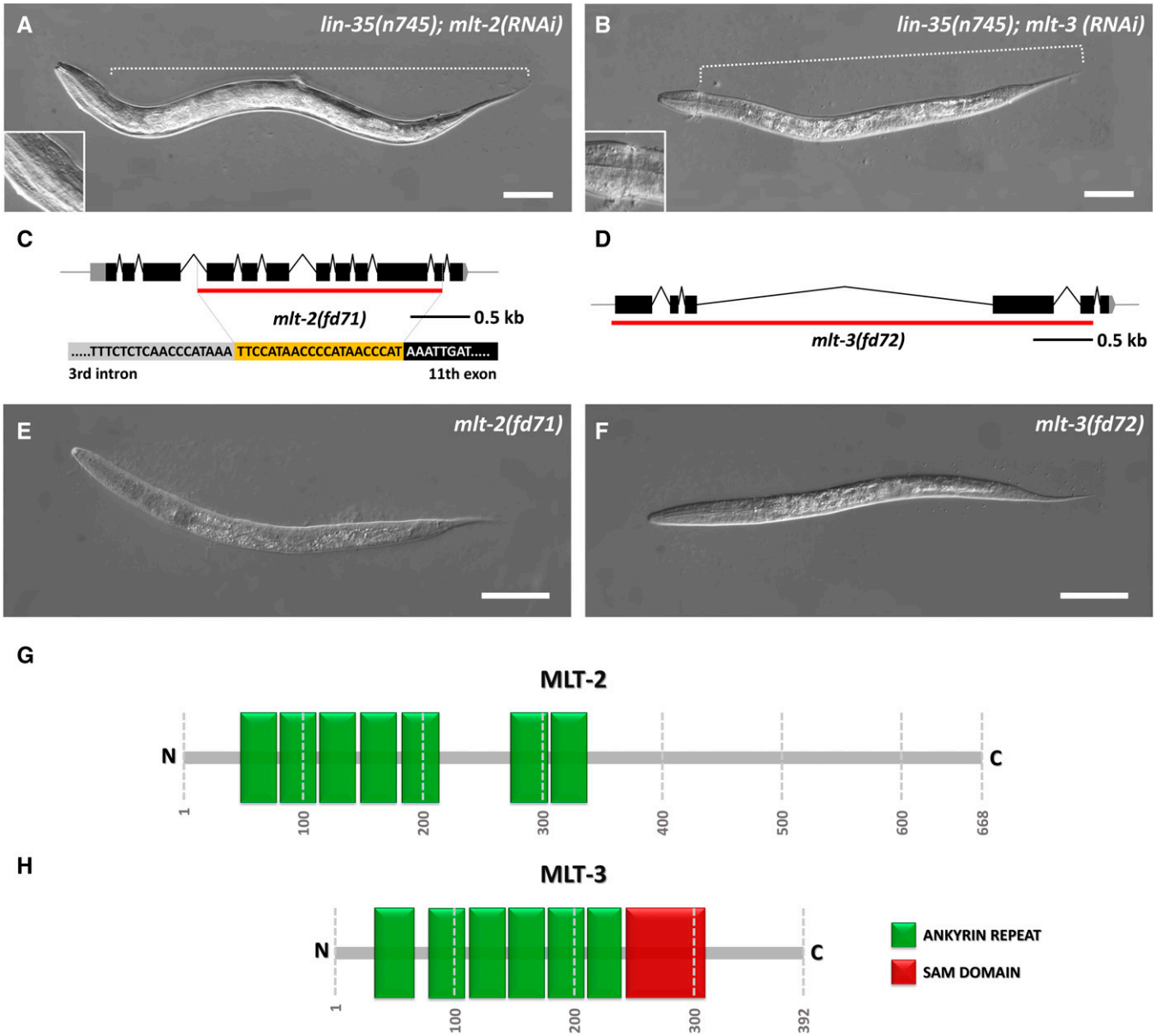

Figure 2 Molting defects in *mlt-2* and *mlt-3* mutants. (A, B) DIC images of *lin-35(n745)* animals, which display partial encasement within old cuticle following *mlt-2(RNAi)* (A) and *mlt-3(RNAi)* (B). Enlargements show constrictions within the head regions. (C, D) Schematic representations of *mlt-2* (C) and *mlt-3* (D); red lines indicate deleted regions in *mlt-2(fd71)* (C) and *mlt-3(fd72)* (D). The yellow region in (C) represents the inserted oligonucleotide that replaces the deleted region of *mlt-2(fd71)*. (E, F) DIC images of homozygous *mlt-2(fd71)* (E) and *mlt-3(fd72)* (F) deletion mutants. (G, H) Schematic illustration of MLT-2 (G) and MLT-3 (H) proteins with annotated predicted ankyrin repeats (green boxes) and SAM domain (red box). Numbers specify positions of amino acids. Bar, 50 μm (A, B, E, and F).

stain, which was added to levamisole to a final concentration of 0.2 μg/μl.

RNA interference

RNAi was performed using bacterial strains from Geneservice library. The standard feeding protocol was followed (Ahringer 2005). Because *mlt-2*(*RNAi*) does not cause molting defects in nonsensitized backgrounds, marker localization studies involving *mlt-2*(*RNAi*) were carried out using strains that were previously grown for one or two generations on *lin-35(RNAi)* plates, which increases RNAi susceptibility (Wang *et al.* 2005); this procedure was used for *mlt-3(RNAi)*, although partially penetrant molting defects were observed for *mlt-3(RNAi)* in wild-type backgrounds. *lin-35(RNAi)* presensitization was not performed in other experiments. For the *mlt-4(sv9)* enhancement study, animals were fed with *nekl-2(RNAi)* or *nekl-3(RNAi)* for several generations prior to evaluation. Their progeny were then synchronized and analyzed after 2 days. *gfp(RNAi)* was used as an RNAi control except for experiments involving *gfp*::*chc-1*, in which case strains

carrying pPD129.36 were used; pPD129.36 expresses an ~200-bp dsRNA sequence that is not homologous to any *C. elegans* gene (Timmons *et al.* 2001).

Genetic mosaic analyses

Genetic mosaic analyses were performed using previously described methods (Yochem *et al.* 1998, 2000, 2006). Only healthy L4 and young adult mosaic animals were analyzed. Strains used in this study were SP2734, WY1098, and WY1117.

CRISPR-Cas9 generation of mlt-2 and mlt-3 deletion alleles

Using the CRISPR design tool (http://crispr.mit.edu), *mlt-2* and *mlt-3* sequences with high scores were chosen in regions close to the start and stop codons. Selected sequences were used for designing primers for site-directed mutagenesis to insert specific sequences into pDD162 (*Peft-3*::*Cas9* + empty sgRNA) using the Q5 Site-Directed Mutagenesis Kit (New England Biolabs, Beverly, MA). Primers used in these experiments included *mlt-2* 5′ forward, 5′-taacacttg catgtgcggggttttagagctagaaatagcaagt-3′; *mlt-2* 3′ forward, 5′-ataattccgtaaagcctgggttttagagctagaaatagcaagt-3′; *mlt-3* 5′ forward 1, 5′-tattgccagatctactcgagttttagagctagaaatagcaagt-3′; *mlt-3* 5′ forward 2, 5′-gatggaacatatgtgactcgttttagagc tagaaatagcaagt-3′; *mlt-3* 3′ forward 1, 5′- ctctggagagcttag gatcgttttagagctagaaatagcaagt-3′; *mlt-3* 3′ forward 2, 5′-gagagcttaggatccggtcgttttagagctagaaatagcaagt-3′; and universal reverse, 5′-caagacatctcgcaatagg-3′.

Animals were injected with pDD162 derivatives and the pTG96 co-injection marker. Green F_1 progeny were allowed to lay eggs before they were lysed and their genomic DNA was used for PCR screening for deletions. Because *mlt-2* and *mlt-3* are essential, viable heterozygotes were injected with appropriate fosmids and pTG96. For *mlt-2* rescue, a mix of five fosmids was used: *WRM0610dG01*; *WRM0618cD05*; *WRM0620bC01*; *WRM0636cH02*; and *WRM0633bB08*. *mlt-3* rescue was performed with fosmid *WRM0610dD02*. Candidate rescued homozygous strains were confirmed and characterized by DNA sequence analysis.

CRISPR-Cas9 generation of nucleotide substitutions

To generate *nekl-2* hypomorphic alleles, genomic substitutions were made using the coconversion strategy for the induction of point mutations (Arribere *et al.* 2014; Paix *et al.* 2014). Briefly, pJA42 (Cas9 + *rol-6* sgRNA construct) and *rol-6(gof)* donor ssDNA were co-injected with appropriate pDD162 derivatives and ssDNAs to create point mutations in desired genes. The following primers were used for site-directed mutagenesis of pDD162: *nekl-2(fd88)* forward, 5′-tcgaacctccaccgacggataaggtaatttttaattg-3′; *nekl-2(fd79)/(fd81)/(fd83)/(fd84)/(fd89)/(fd90)/(fd91)* forward, 5′-ttatgcagtacgcggaagggttttagagctagaaatagcaagt-3′; universal reverse, 5′-caagacatctcgcaatagg-3′. Repair oligos containing the desired mutations, together with novel restriction sites used for screening included *nekl-2(fd88)*, ttgttcttccctatttgatatcaattcattgcgatttgggaagaatcgaagctagcacgac ggataaggtaatttttaattgtattagtgttttgatttagagaaaaat; *nekl-2(fd79)*, gtaaatttaattttaaaattgaattaaaattcgatatgttcagttatgcagctggcggaa catcacacattagagagattaataaatgatcagagagcgattaaagattcaaacatga; *nekl-2(fd81)*, attttaaaattgaattaaaattcgatatgttcagttatgcagtacgcg gaacatgccacattagagctcttaataaatgatcagagagcgattaaagattcaaacat gagagaatatttt; *nekl-2(fd83)*, gtaaatttaattttaaaattgaattaaaattcgatatg ttcagttatgcagctggcggaaggacaaacattagagagattaataaatgatcagaga gcgattaaagattcaaacatga; *nekl-2(fd84)*, attttaaaattgaattaaaattc gatatgttcagttatgcagtacgcggaacatgccacattagagctcttaataaatgatca gagagcgattaaagattcaaacatgagagaatatttt; *nekl-2(fd89)*, gtaaatttaatt ttaaaattgaattaaaattcgatatgttcagttatgcagctggcggaagcacaaaca ttagagagattaataaatgatcagagagcgattaaagattcaaacatga; *nekl-2(fd90)*, gtaaatttaattttaaaattgaattaaaattcgatatgttcagttatgcagctggcggaag cagcaacattagagagattaataaatgatcagagagcgattaaagattcaaacatga; and *nekl-2(fd91)*, gtaaatttaattttaaaattgaattaaaattcgatatgttcagtta tgcagctggcggaagcaggaacattagagagattaataaatgatcagagagcgattaaa gattcaaacatga. The introduced restriction sites were as follows: *Nhe*I for *nekl-2(fd88)*, *Pvu*II for *nekl-2(fd79)/(fd81)/(fd83)/(fd89)/(fd90)/(fd91)*, and *Sac*I for *nekl-2(fd84)*.

F_1 progeny of injected animals were selected for the Rol phenotype, were allowed to lay eggs, and were then screened by single-worm PCR and restriction enzyme analysis to identify candidate heterozygotes containing the desired mutations. F_2 progeny were screened as above, and, in the case of homozygous-lethal alleles, heterozygotes were injected with a *nekl-2(+)* construct (pDF166) and pTG96 to obtain homozygous rescued lines. All homozygous lines were confirmed by sequencing.

CRISPR-Cas9 generation of fluorescently tagged proteins

C-terminal fluorophore::3×Flag insertions were created using Cas9-mediated homologous recombination using the self-excising selection cassette method (Dickinson *et al.* 2015). pDD162-based constructs expressing Cas9 and sgRNAs were generated using Q5 Site-Directed Mutagenesis Kit and the following primers: *nekl-2* forward, 5′-ttgcccacttccgaat gatgttttagagctagaaatagcaagt-3′; *nekl-3* forward, 5′-ggagtt gttgattggtcccgttttagagctagaaatagcaagt-3′; *mlt-4* forward, 5′-ctcaaattcggtgctccgagttttagagctagaaatagcaagt-3′; universal reverse, 5′-caagacatctcgcaatagg-3′. For *mlt-2* and *mlt-3*, the same 3′ Cas9-sgRNA constructs were used in the generation of *mlt-2* and *mlt-3* deletion alleles. Repair templates were created by inserting homology arms into *Avr*II- and *Spe*I-digested fluorophore-containing plasmids pDD268 (NeonGreen::3×Flag), pDD282 (gfp::3×Flag), and pDD285 (mKate2::3×Flag). Homology arms were either PCR amplified (~700 bp) or ordered as gene blocks (440 bp) and inserted into constructs using NEBuilder HiFi DNA Assembly (New England Biolabs), which uses modified Gibson assembly methods. Homology arm PCR amplification primers were as follows: *mlt-2* 5′ arm forward, 5′-acgttg taaaacgacggccagtcgccggcacaggaatgccaaagttttgctg-3′ and reverse, 5′-catcgatgctcctgaggctcccgatgctcccagtgatcggctaaga attgc-3′; *mlt-3* 3′ arm forward, 5′-cgtgattacaaggatgacgatgacaa

gagatgattttaatttttttttttgagaaag-3′ and reverse, 5′-ggaaacagctat gaccatgttatcgatttcgccccagaatgaatttctatg-3′; *nekl-2* 5′ arm forward, 5′-acgttgtaaaacgacggccagtcgccggcacttacttaaaacacacac gga-3′ and reverse, 5′-catcgatgctcctgaggctcccgatgctccatacttt gaatgcacttgact-3′; *nekl-3* 3′ arm forward, 5′-cgtgattacaaggat gacgatgacaagagataaaaaaagctataacatttcaatttc-3′ and reverse, 5′-ggaaacagctatgaccatgttatcgatttcaatgtggcaaacacagtgtta-3′. PAM sites were mutated in repair templates, without amino acid changes. The presence of the homology arms was confirmed by sequencing. Co-injection markers were pTG96 and pCFJ90 (*Pmyo-2*::*mCherry*), and selection was based on the Rol phenotype and resistance to Hygromycin B. Positive homozygous animals were heat shocked at 32° for 4–6 h to activate the Cre recombinase, which removes the self-excising selection cassette flanked by *LoxP* sites. PCR amplification confirmed the presence of insertions within desired genes.

Yeast two-hybrid analysis

Identification of physical interactions between NEKL-3 and MLT-3 was performed using the ProQuest Two-Hybrid System (Invitrogen, Carlsbad, CA). The gateway cloning system was used to generate entry clones, bait, and prey plasmids. To generate entry clones, *nekl-3* cDNA was amplified using 5′-ggggacaagtttgtacaaaaaagcaggcttcatggacaaaatttcgaacatcta-3′ and 5′-ggggaccactttgtacaagaaagctgggtcttagaattgcgttgaaggagttgtt-3′ primers, whereas *mlt-3* amplification was accomplished with 5′-ggggacaagtttgtacaaaaaagcaggcttcatgtcgtttcgtgtccgtttttc-3′ and 5′- ggggaccactttgtacaagaaagctgggtctcaaacatgtgaggaaacttttaaa-3′ primers. The BP clonase recombination reaction between cDNA clones and pDONR221 was used to create entry vectors, which were used in the LR clonase recombination reaction with the bait destination vector pDEST32 and prey destination vector pDEST22. All constructs were sequenced to confirm the presence of the correct insert. Yeast strain MaV203 was cotransformed with all possible combinations of *nekl-3*/*mlt-3*/control empty vector bait and *nekl-3*/*mlt-3*/control empty vector prey constructs. Strains were tested for HIS3 self-activation by addition of 3-amino-1,2,4-triazole (3-AT) to SC-Leu-Trp-His medium. After the HIS3 self-activation threshold was determined, yeast strains were tested for their ability to grow on selective media SC-Leu-Trp-Ura, SC-Leu-Trp-His + 3-AT, and SC-Leu-Trp + 5-fluoroorotic acid (5-FOA). LacZ /β-gal activity was determined using chlorophenol red-β-D-galactopyranoside (CPRG) as a substrate. β-gal activity was determined as follows: β-gal units = (1000 × absorbance at 574 nm)/[(duration of reaction) × (sample volume) × (absorbance at 600 nm)]. Control constructs were provided by the manufacturer, including pEXP32/Krev1 bait (same for all controls), pEXP22/RalGDS-wt prey (for strong positive control), pEXP22/RalGDS-m1 prey (for weak positive control), and pEXP22/RalGDS-m2 prey (for negative control).

Data availability

The authors state that all data necessary for confirming the conclusions presented in the article are represented fully within the article. Reagents or specific data from this manuscript available upon request.

Results

C. elegans mlt-4 is required for normal molting and encodes a conserved ankyrin repeat protein

The *sv9* allele was identified in a screen for recessive mutations that affect the completion of molting. Homozygous *sv9* mutants typically arrest as L2- to L3-stage larvae, after failing to shed portions of old cuticle during molting cycles. In most *sv9* homozygotes, the central body and tail regions are trapped within two layers of cuticle, whereas the head region contains only a single layer (Figure 1A). Other *sv9* homozygotes display the "corset" phenotype in which both the head and tail regions are free of old cuticle (Figure 1B), similar to what is observed for *nekl-3(sv3)* mutants (Yochem *et al.* 2015).

sv9 was mapped to a region on LG V, and microinjection of cosmid ZC15, which contains a genomic insert corresponding to a portion of the implicated region, fully rescued the *sv9* molting defect (see *Materials and Methods*). *sv9* was subsequently rescued by a single open reading frame, ZC15.7 (hereafter referred to as *mlt-4*). Sequencing of the *mlt-4* locus in *sv9* mutants revealed a single G-to-A transition of the final nucleotide of the fifth intron (Figure 1C). This mutation affects the highly conserved G of the canonical 3′ splice acceptor site (TTTTCAG) and may reduce or eliminate incorporation of exon 6 into the mature *mlt-4* mRNA. We note that *mlt-4* activity was largely recalcitrant to RNAi and thus was not used in this study.

We also obtained a putative null deletion allele of *mlt-4* (*tm1484*) (The *C. elegans* Deletion Mutant Consortium 2012), which contains a 637 bp in frame deletion, including 187 bp upstream from the start codon (Figure 1C). This deletion completely eliminates the 5′ UTR, the first exon, and most of the first intron of *mlt-4*. *mlt-4(tm1484)* homozygotes display 100% larval lethality, consistent with a strong loss-of-function or null mutation. We also examined the F1 progeny from eight germline-mosaic *mlt-4(tm1484)* mothers and observed complete encasement within old cuticle at the L1/L2 molt (n = 435).

The *mlt-4* mRNA is derived from nine exons (Figure 1C) and encodes a predicted 624-aa protein. Using 5′ RACE, we determined that the *mlt-4* mRNA begins 38 nucleotides upstream of the presumed AUG start codon and lacks a *trans*-spliced leader. Moreover, alternative forms of the *mlt-4* mRNA are not abundant (also see WormBase). The predicted MLT-4 protein contains 13 tandem copies of an ankyrin repeat domain (Figure 1D). Splicing from exon 5 to exon 7 in *sv9* mutants would be predicted to eliminate the fifth ankyrin repeat, as well as parts of the fourth and sixth repeats, but would not induce a frameshift. Ankyrin repeat domains are important for protein–protein interactions and can serve as molecular scaffolds (Mosavi *et al.* 2004; Voronin and Kiseleva 2008; Hollenbeck *et al.* 2012). Based on reciprocal BLAST and OrthoList (Shaye and Greenwald 2011),

MLT-4 is orthologous to human inversin (INVS), and more similar in amino acid sequence than a previously reported INVS ortholog, NPHP-2 (Figure S1 and Figure S2) (Warburton-Pitt *et al.* 2012). Unlike MLT-4, however, INVS contains a C-terminal region that is largely intrinsically disordered. Although specific amino acid sequences within this region are not highly conserved in mammals, MLT-4 lacks the C-terminal region of mammalian INVS proteins altogether (Figure S1). Also unlike MLT-4, INVS contains two predicted IQ domains, which are implicated in Ca^{2+}-independent calmodulin binding (Rhoads and Friedberg 1997).

The conserved ankyrin repeat proteins MLT-2 and MLT-3 are essential for normal molting

The *C. elegans* genome is predicted to encode ~13 proteins with sequence similarity to MLT-4/INVS, most of which contain ankyrin repeats (Figure S2 and Table S1). To determine if any of these proteins play a role in the regulation of molting, we carried out RNAi against each gene in two RNAi-hyper-sensitive strains [*lin-35(n745)* and *rrf-3(pk1426)*] and scored for molting defects. Notably, downregulation of two genes, C01H6.2 and Y39C12A.1, led to partial entrapment within old cuticle, which can occur at any of the four molting stages (Figure 2, A and B, Table S1, and data not shown). We hereafter refer to C01H6.2 as *mlt-2* and Y39C12A.1 as *mlt-3*.

mlt-2 encodes a predicted protein of 668 aa with seven N-terminal ankyrin repeat domains along with a C-terminal region that is structurally uncharacterized (Figure 2G). Several human proteins are similar to MLT-2, including the annotated ortholog ANKS6 (Shaye and Greenwald 2011) (Figure S1). Unlike MLT-2, however, ANKS6 contains a C-terminal sterile alpha motif (SAM) domain, which is implicated in both protein and RNA interactions (Kim and Bowie 2003). *mlt-3* encodes a predicted 392-aa protein with six N-terminal ankyrin repeat domains and one C-terminal SAM domain (Figure 2H) and is orthologous to mammalian ANKS3 (Figure S1) (Shaye and Greenwald 2011).

Using CRISPR-Cas9 methods, we generated deletion alleles for both *mlt-2* and *mlt-3*. *fd71* contains an indel in which 2051 nucleotides spanning exons 4–11 of *mlt-2* were deleted and replaced with a 21-bp insertion (Figure 2C). *fd72* contains a 4028-nucleotide deletion, which removes approximately the first five exons of *mlt-3* (Figure 2D). One hundred percent of homozygous *mlt-2(fd71)* and *mlt-3(fd72)* mutants arrested as L1–L2 larvae that were fully encased within two layers of cuticle (Figure 2, E and F), similar to what we observed for null deletion alleles of *nekl-2* and *nekl-3* (Yochem *et al.* 2015). Notably, the phenotypes of *mlt-2(fd71)*; *mlt-3(fd72)* and *mlt-2(fd71)*; *mlt-4(tm1484)* double mutants did not differ from the phenotypes observed in the single mutants (data not shown). Likewise, *nekl-2(gk839)*; *nekl-3(gk506)* double null mutants showed identical phenotypes to single mutants (data not shown). Furthermore, the phenotypes of *mlt-2(fd71)*, *mlt-3(fd72)*, or *mlt-4(tm1484)* alleles were not enhanced by RNAi of *mlt-2*, *mlt-3*, *nekl-2*, or *nekl-3* (data not shown). These results indicate that the MLTs and NEKLs do not have redundant functions earlier in development. Collectively, our findings demonstrate that conserved ankyrin repeat proteins are specifically required for the completion of molting in *C. elegans*.

mlt-2, mlt-3, and mlt-4 are required in the epidermal hyp7 syncytium

To elucidate the cell types in which *mlt-2*, *mlt-3*, and *mlt-4* activities are essential, we carried out genetic mosaic analyses using standard methods (Yochem *et al.* 1998, 2000, 2006). For these studies, mutant strains containing GFP-marked *mlt(+)* rescuing extrachromosomal arrays were analyzed for array inheritance within the cell lineages of viable young adults or L4 larvae. The absence of the rescuing array within a specific cell lineage in aphenotypic animals implies that gene function is not required within that lineage or its derived tissues. Notably, this analysis implicated *mlt-2*, *mlt-3*, and *mlt-4* as being specifically required in the hyp7 epidermal syncytium, a large multinucleate cell that covers most of the midbody of the worm. A series of cell fusion events during embryonic and postembryonic development generate hyp7, with contributions coming from the ABa, Abp, and C blastomeres (Sulston *et al.* 1983). Thus, segregation of the array within any one of these founder cells can be sufficient to rescue a gene requirement within hyp7.

In the case of *mlt-2*, *mlt-3*, and *mlt-4* mutants, we observed that the presence of rescuing arrays within only ABa or ABp was able to fully suppress molting defects (Figure 3A). Moreover, in the case of *mlt-4*, viable adults were identified that contained positive clones in only ABarp (two mosaics), ABarpaa (one mosaic), or ABplapa (one mosaic). Correspondingly, the presence of a rescuing array within C only was able to rescue molting defects in all three *mlt* mutants (Figure 3A). Because the hyp7 syncytium is derived exclusively from descendants of the ABa, ABp, and C lineages, the most straightforward interpretation is that *mlt-2*, *mlt-3*, and *mlt-4* are specifically required in hyp7, consistent with previous findings for *nekl-2* and *nekl-3* (Yochem *et al.* 2015). Furthermore, mosaic analyses indicated that there is no maternal requirement or functional contribution of *mlt-2*, *mlt-3*, or *mlt-4*. Namely, the progeny of animals in which rescuing arrays were absent from the maternal germline arrested with molting defects at the same developmental stage as (array-minus) mutants derived from germline-positive adults (Figure 3B). This finding is consistent with previous results for *nekl-2* and *nekl-3* and indicates that neither the NEKL nor MLT proteins play a critical role during embryogenesis. We note, however, that our results do not preclude a nonessential role for MLT and NEKL proteins in other epidermal syncytia.

Fluorescently tagged MLT-2, MLT-3, and MLT-4 proteins are expressed in the epidermis and show dynamic movement within puncta

To determine the tissue and subcellular expression patterns of MLT-2, MLT-3, and MLT-4, we used CRISPR-Cas9 methods to add fluorescent tags to the endogenous loci. Expression of all

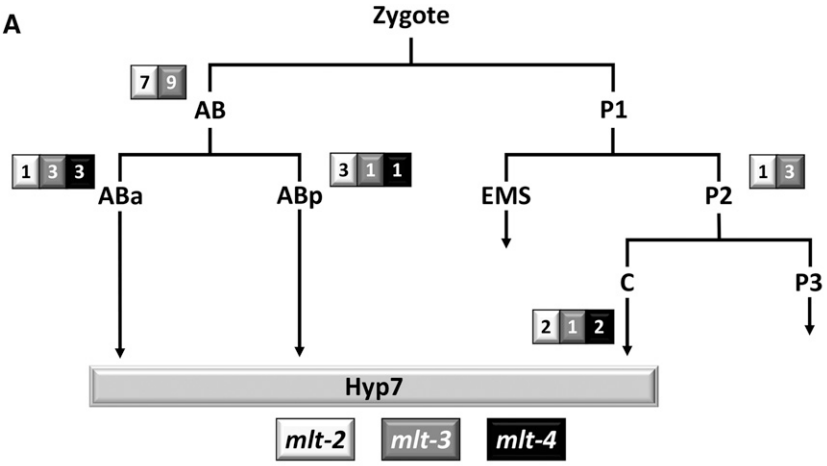

B

Germline mosaics	P_0 Germline mosaics	F_1 Embryonic lethal	F_1 Larval lethal	F_1 Adults	F_1 Total
mlt-2(fd71)	5	3	489	0	492
mlt-3(fd72)	3	5	346	0	351
mlt-4(sv9)	7	4	1081	0	1085

Figure 3 Mosaic analysis of *mlt genes*. (A) The early cell lineage of *C. elegans* is depicted showing contributions of ABa, ABp, and C to the epidermal syncytium, hyp7. The number of viable adult mosaic animals in which the rescuing array was present exclusively within AB, ABa, ABp, P2, or C in *mlt-2(fd71)*, *mlt-3(fd72)*, and *mlt-4(sv9)* mutants is shown in the adjacent boxes. For each mutant, the only descendant common to all the identified mosaic animals was hyp7. (B) Summary of phenotypes for the F_1 progeny of *mlt-2*, *mlt-3*, and *mlt-4* germline-mosaic animals. In all cases, larvae arrested with molting defects and no maternal contribution was observed.

three genes was detected exclusively within the epidermis, including hyp7, beginning in late embryogenesis (Figure 4A and data not shown). MLT-2::mKate2 and MLT-4::GFP displayed similar patterns of expression at the epidermal apical surface within well-separated puncta and also showed strong accumulation at the boundary of hyp7 and seam cells. In more medial planes, both MLT-2 and MLT-4 were more evenly dispersed throughout the cytosol with reduced accumulation at the seam cell boundary (Figure 4A). In contrast, accumulation of MLT-3::mKate2 was not highly enriched at the hyp7–seam cell boundary (Figure 4A and data not shown). Like MLT-2 and MLT-4, MLT-3 was expressed in apical puncta, although its expression was stronger and typically more dispersed than that observed for MLT-2 and MLT-4 (Figure 4A). In medial planes, expression of MLT-2, MLT-3, and MLT-4 was largely excluded from nuclei, but in some cases the tagged proteins exhibited partial enrichment or exclusion within other smaller compartments (Figure 4A). We note that animals homozygous for the modified *mlt-3*::*mKate2* locus displayed a partially penetrant molting-defective phenotype, suggesting that fluorophore insertion may have slightly impaired the activity of the endogenous *mlt-3* gene.

To determine the extent of expression overlap between MLT-2, MLT-3, and MLT-4, we constructed doubly marked strains. Extensive colocalization was observed between MLT-2::mKate2 and MLT-4::GFP at apical puncta and at the hyp7–seam cell boundary, although some nonoverlapping puncta were also observed (Figure 4B). In addition, we noticed that MLT-2::mKate2 had some tendency to form larger accumulations, which were not observed for MLT-4::GFP (Figure 4, A and B and data not shown). In contrast to MLT-2 and MLT-4, MLT-3::mKate2 and MLT-4::GFP signals did not overlap significantly (Figure 4B). Taken together, our expression data are consistent with roles for MLT-2, MLT-3, and MLT-4 in the epidermis and suggest that MLT-2 and MLT-4 may have closely connected cellular functions.

Notably, all three MLT reporters were visible as highly dynamic structures in the epidermis (Figure 4C, File S1, File S2, File S3, File S4, File S5, and data not shown). In general, larger accumulations were less mobile and displayed short oscillating or linear movements, or no motility, within the time frame of the analysis (25–50 sec). In contrast, numerous smaller puncta throughout hyp7 displayed rapid linear and circular dynamics but were hard to trace given their movement in and out of the focal plane. We observed that smaller puncta in some cases branch out from larger accumulations or merge between each other and with bigger puncta. A high level of motility was observed at the hyp7–seam cell boundary region for all three MLTs including MLT-3::mKate2, which was not highly enriched in this region. Where possible, we quantified average velocities of puncta that were moving within a single horizontal plane, which included mostly oscillating larger puncta at the apical surface. For MLT-2::mKate2 the average velocity of puncta was 43.7 nm/sec, ranging from 13.3 to 117 nm/sec (51 puncta, eight animals). MLT-3::mKate2 had an average velocity of 59.2 nm/sec, ranging from 40.3 to 80.9 nm/sec (16 puncta, four animals). MLT-4::GFP puncta had an average velocity of 68.5 nm/sec, ranging from 29.3 to 139.6 nm/sec (71 puncta, seven animals). We note that particle movement was often erratic within the time frame of our observation and that MLT-puncta

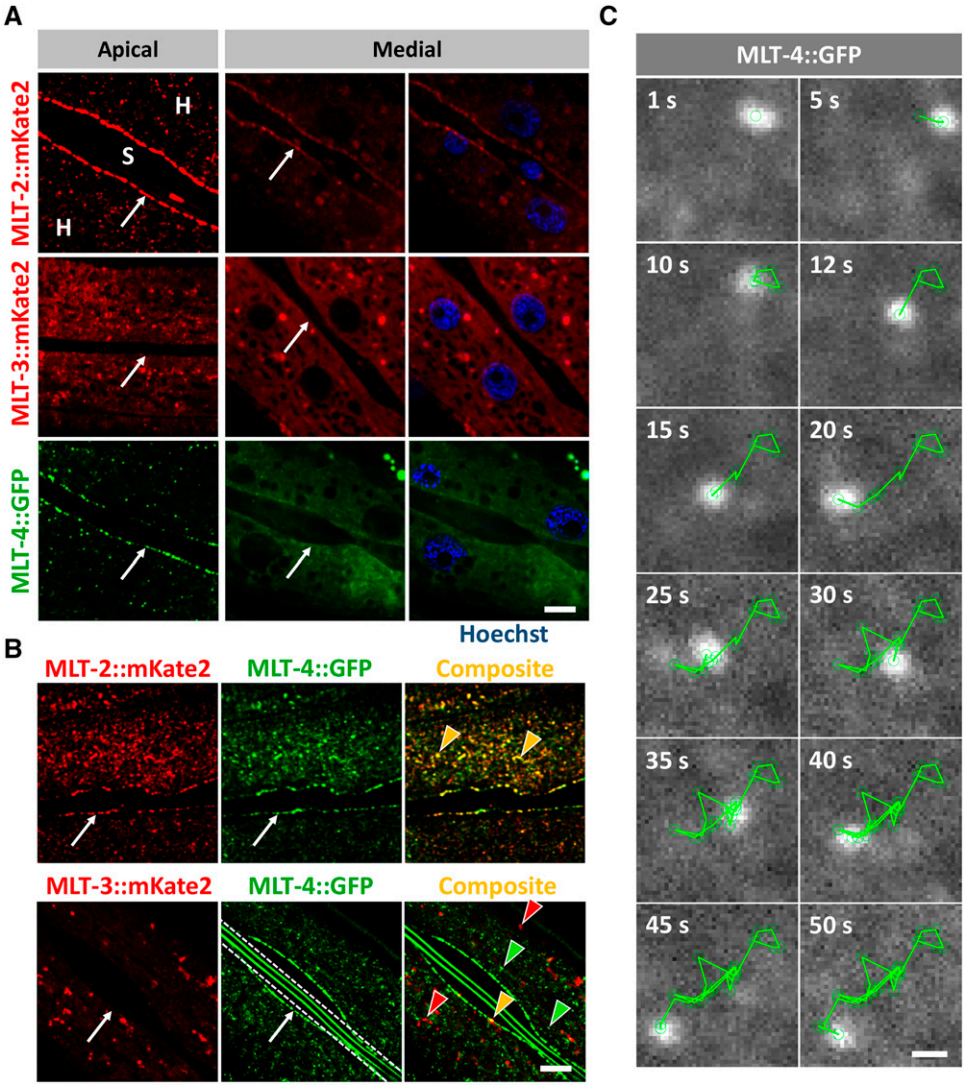

Figure 4 Expression analysis of MLT proteins. (A) Confocal images of fluorescently labeled MLT-2::mKate2, MLT-3::mKate2, and MLT-4::GFP show expression in epidermis. Punctate accumulations were observed near the apical surface of the hyp7 syncytium (H), but not in the neighboring seam cells (S). MLT-2 and MLT-4 also show strong enrichment at the hyp7–seam cell boundary (white arrows). In medial planes, MLT-2, MLT-3, and MLT-4 are largely expressed in the cytosol and are largely absent from nuclei (blue) labeled with Hoechst. Bar, 5 μm. (B) Colocalization analyses revealed extensive overlap between apical puncta of MLT-2::mKate2 and MLT-4::GFP but not MLT-3::mKate2 and MLT-4::GFP. Images in A were modified to remove background fluorescence to highlight expression in puncta. Red and green arrowheads indicate representative puncta that express only one marker, whereas yellow arrowheads indicate colocalization. White arrows indicate hyp7–seam cell boundaries. White dashed lines demarcate autofluorescent alae. Bar, 5 μm. (C) Representative time lapse movie frames of MLT-4::GFP apical puncta. Green line traces the direction of particle movement. Bar, 0.5 μm.

movement was not confined to a single stage but occurred throughout the life cycle of the animal.

Genetic analyses indicate functional cooperation of the NEKL and MLT proteins

The mutant phenotypes of *mlt-2*, *mlt-3*, and *mlt-4* are very similar to those previously described for *nekl-2* and *nekl-3* mutant animals (Yochem *et al.* 2015). To test for functional genetic interactions between the *mlt* and *nekl* genes, it was first necessary to obtain weak hypomorphic alleles of *nekl-2* and *nekl-3*. Specifically, we postulated that viable hypomorphic alleles of *nekl-2* or *nekl-3* may be hyper-sensitive to further inhibition of pathway components, such as the *mlt* genes. We began by testing three aphenotypic alleles of *nekl-2* and four aphenotypic alleles of *nekl-3* generated by the Million Mutation project (Thompson *et al.* 2013). Two of the four tested *nekl-3* alleles (*gk296270* and *gk894345*) were strongly enhanced by *nekl-2(RNAi)*, leading to a fully penetrant larval arrest (Figure 5, A and C). By contrast, *nekl-2(RNAi)* had no effect on wild-type worms (data not shown) and produced only weak-to-moderate effects on the two other *nekl-3* strains tested (*gk774978* and gk296269; Figure 5A). Similar results were also obtained for the four *nekl-3* alleles following *nekl-3(RNAi)* feeding (data not shown). Notably, the most strongly enhanceable *nekl-3* alleles contained amino acid substitutions within the predicted kinase domain (P224L and D228N). In addition, we observed that the level of enhancement roughly corresponded to the degree of conservation at the mutated site. In contrast to *nekl-3*, none of the Million Mutation *nekl-2* alleles showed strong enhancement following RNAi of *nekl-2* or *nekl-3* (Figure 5B), although two strains showed moderate levels of molting defects.

To obtain highly sensitized alleles of *nekl-2* for enhancer analysis, we used CRISPR-Cas9 methods to generate changes in two regions of *nekl-2*. Whereas substitution of a PPP sequence (aa 283–285) outside the predicted kinase domain failed to provide sensitization, changes within a small region of the kinase domain (aa 84–92) led to a spectrum of loss-of-function phenotypes (Figure 5B). In particular, changes at

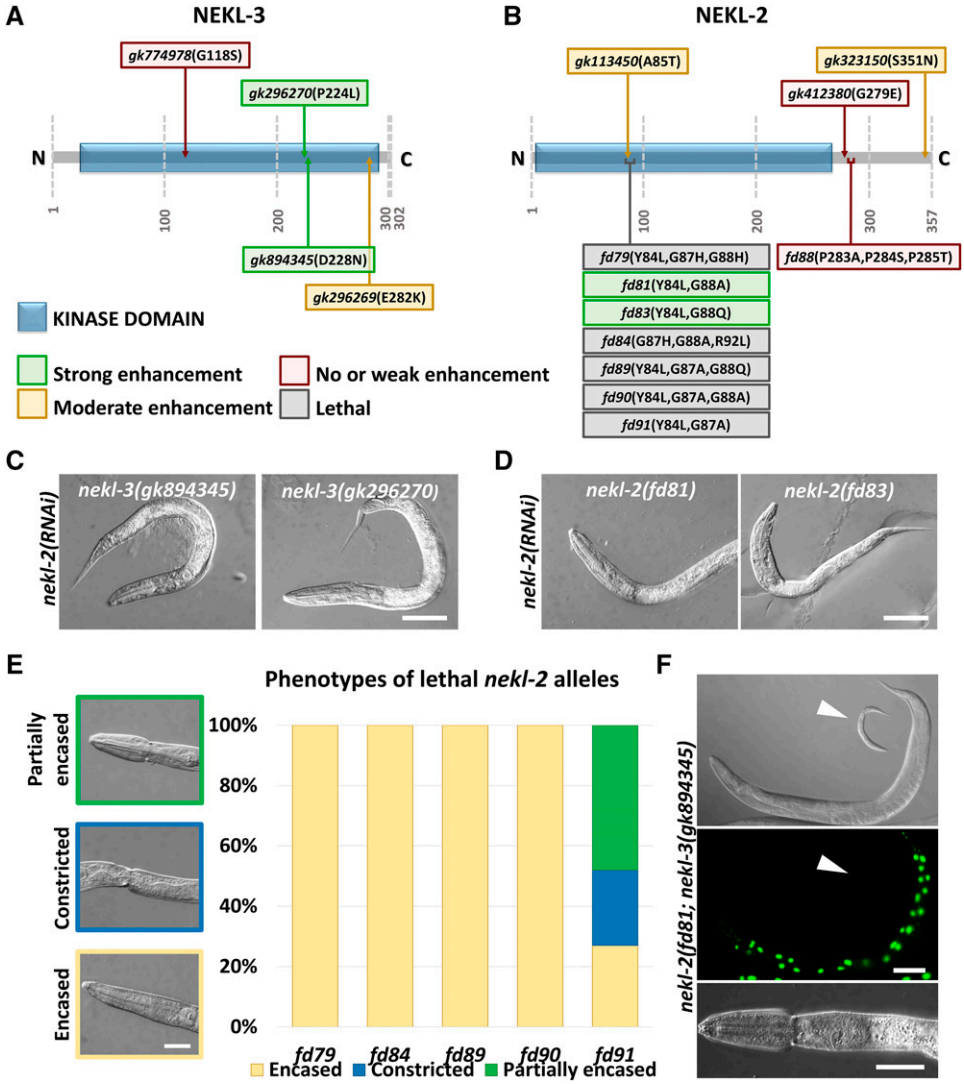

Figure 5 Isolation of *nekl-2* and *nekl-3* hypomorphic alleles. (A, B) Schematic representations of NEKL-3 (A) and NEKL-2 (B) proteins, with annotated predicted kinase domains (blue boxes). Mutant alleles indicated by text boxes, which are color coded according to the severity of the mutation: green, strong enhancement; yellow, moderate enhancement; red, no or weak enhancement; gray, homozygous lethal. (C, D) Representative DIC images of select *nekl-3* (C) and *nekl-2* (D) hypomorphic alleles treated with *nekl-2(RNAi)*, which led to early larval lethality and molting defects. Bar, 50 μm. (E) Phenotypic analysis of homozygous-lethal *nekl-2* alleles. Whereas *fd79*, *fd84*, *fd89*, and *fd90* displayed early arrest with complete encasement, most *fd91* homozygotes were partially encased and arrested later in development (n = 100 for each allele). Bar, 25 μm. (F) *nekl-2(fd91)*; *nekl-3(gk894345)* double mutants (GFP^{-}; white arrowhead) arrest as larvae with molting defects, including the corset phenotype (bottom panel). A GFP^{+} worm containing a *nekl-3*$^{+}$ rescuing array (*fdEx286*), which is viable, is shown in the top two panels. Top bar, 100 μm, Bottom bar, 25 μm.

glycines G87 and G88, together with changes at Y84, produced phenotypes ranging from uniform early larval lethality to worms that were largely aphenotypic but strongly enhanced by RNAi of *nekl-2* or *nekl-3* (Figure 5, B, D, and E and data not shown). Common to the homozygous-lethal alleles were changes at G87 including *fd90* (Y84L, G87A, G88A) and *fd84* (G87H, G88A, R92L), which led to arrest at the L1–L2 transition, and *fd91* (Y84L, G87A), which led to arrest in late L2 or early L3 (Figure 5E). In contrast, changes affecting G88 [*fd81* (Y84L, G88A) and *fd83* (Y84L, G88Q)] did not produce lethality but led to strains that were highly sensitive to *nekl-2* or *nekl-3* RNAi feeding (Figure 5, B and D). Moreover, animals homozygous for hypomorphic alleles of both *nekl-2(fd81)* and *nekl-3(gk894345)* arrested at high frequency during larval development (98.5%, n = 1721) and displayed molting defects (Figure 5F), consistent with our previous studies indicating that *nekl-2* and *nekl-3* have functional overlap (Yochem *et al.* 2015).

Both G87 and G88 are completely conserved among NEKL-2/NEK8 orthologs and are largely conserved among members of the NIMA kinase family (Figure S3). To understand the basis for the differential effects of the G87 and G88 mutations, we carried out a computational structural analysis of wild-type NEKL-2 along with the *fd91* (Y84L, G87A) and *fd81* (Y84L, G88A) variants. Structural models predict that the more severe G87A substitution should cause much more extensive changes in intramolecular contacts as compared with the G88A substitution (Figure S4A). These changes are also reflected in the predicted surface structure of the protein, where residue 87 of the G87A variant is much less exposed than the equivalent residue in either wild type or the G88A variant (Figure S4B). Notably, the YAEG sequence is predicted to form an SH2 domain, and thus alterations in G87 may interfere with protein–protein interactions. In contrast, G88 is adjacent to the predicted ATP-binding pocket, and G88A may therefore exert a weak effect on the enzymatic activity of NEKL-2.

The hypomorphic alleles *nekl-2(fd81)* and *nekl-3(gk894345)*, together with a wild-type control, were used to test for

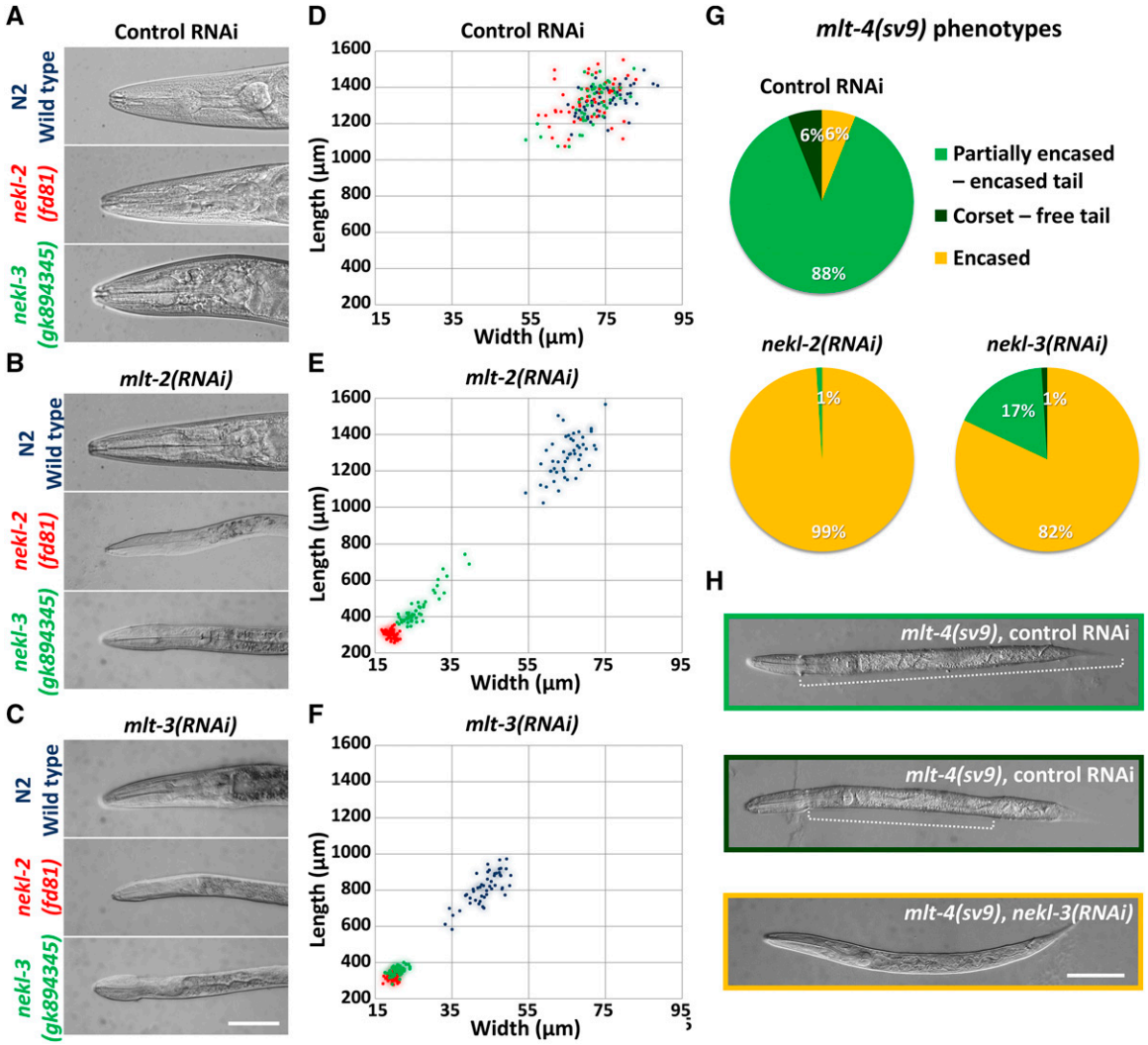

Figure 6 Genetic enhancer analysis of *mlt* and *nekl* genes. (A–C) DIC images of wild-type, *nekl-2(fd81)*, and *nekl-3(gk894345)* strains treated with control *gfp(RNAi)* (A), *mlt-2(RNAi)* (B), or *mlt-3(RNAi)* (C). Note that *mlt-2(RNAi)* and *mlt-3(RNAi)* induce molting defects and larval arrest in *nekl-2(fd81)* and *nekl-3(gk894345)* backgrounds but not in wild type. (D–F) Graphic representation of animal dimensions after RNAi treatment in different genetic backgrounds. Coordinates on the *x* axis indicate body width, whereas coordinates on the *y* axis represent body length. Each animal (n = 50 for each genotype and treatment) is represented by a colored dot corresponding to genotypes in A–C; blue, wild type; red, *nekl-2(fd81)*; green, *nekl-3(gk894345)*. Control *gfp(RNAi)* (D) had no effect on size, whereas RNAi for *mlt-2* (E) or *mlt-3* (F) caused *nekl-2* and *nekl-3* hypomorphs to have much smaller body dimensions as compared with stage-matched wild-type animals. (G) The severity of molting defects in *mlt-4(sv9)* homozygotes is enhanced by *nekl-2(RNAi)* and *nekl-3(RNAi)* treatment relative to the *gfp(RNAi)* control. (H) Representative DIC images of phenotypes described in G. Dotted lines mark the constricted region in partially encased animals. Bars, 50 µm.

enhancement of molting defects by *mlt-2(RNAi)* and *mlt-3(RNAi)*. Wild-type, *nekl-2(fd81)*, and *nekl-3(gk894345)* animals developed normally on control *gfp(RNAi)* plates (Figure 6A) and displayed indistinguishable body size measurements (Figure 6D and Figure S5). As expected for components of a common network, *mlt-2(RNAi)* strongly enhanced both *nekl-2(fd81)* and *nekl-3(gk894345)* hypomorphic alleles, causing early larval arrest with accompanying molting defects, whereas wild-type worms were unaffected (Figure 6, B and E and Figure S5). Similar enhancer effects were also observed for RNAi of *mlt-3*, although *mlt-3(RNAi)* affected wild-type animals to a greater extent; treated N2 animals usually reached adulthood but were smaller and often displayed egg-laying defects, possibly because of some cuticle retention in the midbody region (Figure 6, C and F and Figure S5).

Because RNAi of *mlt-4* is largely ineffective (data not shown), we took a different approach to determine if *mlt-4* genetically interacts with *nekl-2* or *nekl-3*. As described above, *mlt-4(sv9)* homozygotes show a partially encased or corset phenotype and arrest in late stages of L2 or early L3. This property was used to determine if RNAi of *nekl-2* or *nekl-3* can enhance the severity of the *sv9* phenotype and cause earlier developmental arrest. Indeed, complete encasement became the predominant phenotype in *sv9* homozygotes treated with *nekl-2(RNAi)* or *nekl-3(RNAi)*, a phenotype rarely

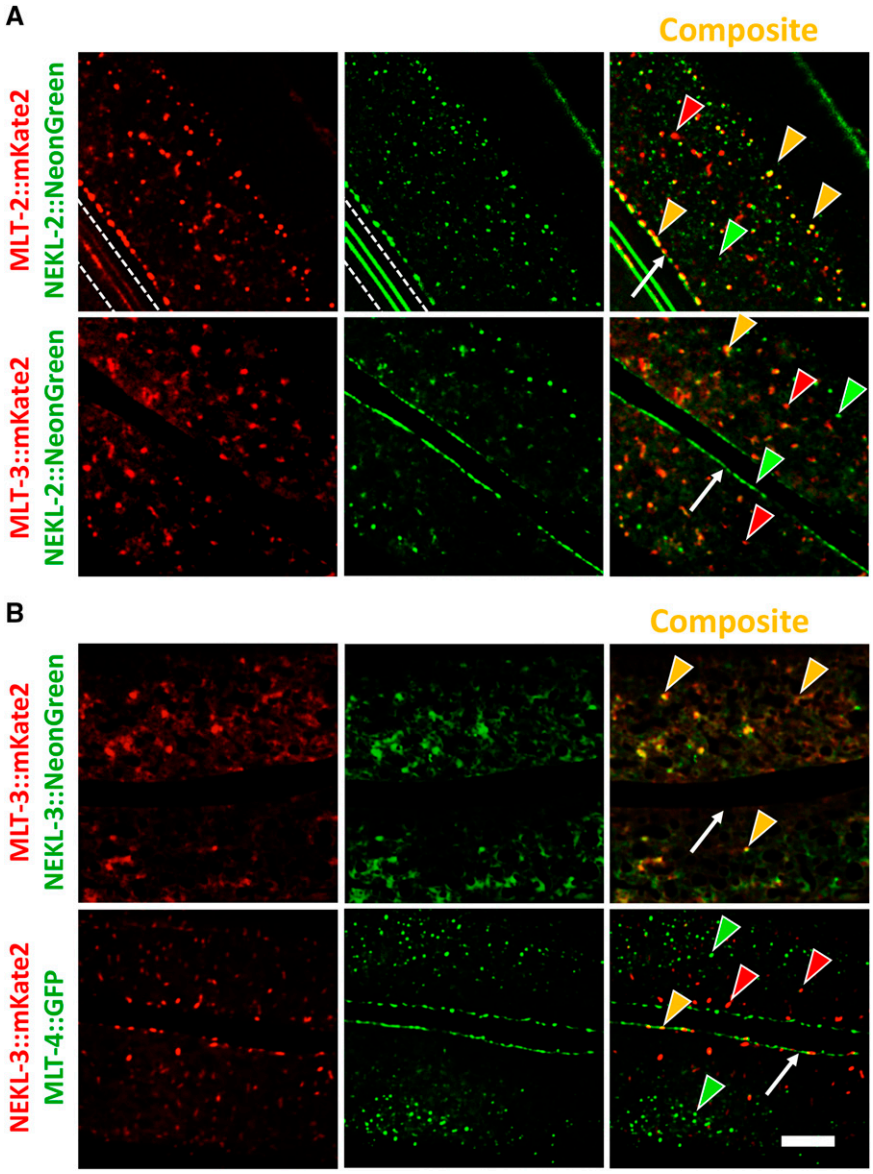

Figure 7 Colocalization of NEKL and MLT proteins. (A) Colocalization analyses of MLT-2::mKate2 and MLT-3::mKate2 with NEKL-2::NeonGreen showing extensive overlap of MLT-2 and NEKL-2 puncta throughout the hyp7 apical surface including the region adjacent to the seam cell. Though less frequent, some NEKL-2 puncta colocalized with MLT-3. White dashed lines in the first two panels demarcate autofluorescent alae. (B) NEKL-3::NeonGreen apical accumulations extensively overlapped with MLT-3::mKate2. In contrast, NEKL-3::mKate2 did not colocalize with MLT-4::GFP puncta. Red and green arrowheads indicate representative puncta that express only one marker, whereas yellow arrowheads indicate colocalization. White arrows indicate hyp7–seam cell boundaries. Bar, 5 μm.

seen with control *gfp(RNAi)* (Figure 6, G and H). Taken together, our genetic analyses implicate the MLT and NEKL proteins in a common pathway or network that controls molting.

Colocalization of NEKL and MLT proteins

We next asked whether NEKL and MLT proteins colocalize in the epidermis. As for the *mlt* genes, we used CRISPR-Cas9 to generate fluorophore-tagged versions of *nekl-2* and *nekl-3*. Consistent with our previous study (Yochem *et al.* 2015), these reporters were expressed strongly within the epidermis beginning in late embryonic development (Figure 7 and data not shown). NEKL-2::NeonGreen was present in cytosolic puncta that were enriched at the hyp7–seam cell boundary, similar to our observations for MLT-2 and MLT-4 (Figure 4A, Figure 7A, and data not shown). As anticipated, NEKL-2::NeonGreen showed extensive colocalization with MLT-2::mKate2 in the apical region of hyp7, although some puncta did not overlap (Figure 7A). In the case of NEKL-2 and MLT-3, coexpression was more variable. In apical regions, including the region encompassing the hyp7–seam cell boundary, most NEKL-2::NeonGreen and MLT-3::mKate2 puncta failed to overlap, although colocalization of some puncta was often observed (Figure 7A). Moreover, in some animals we observed moderate-to-strong overlap, particularly in larger apical accumulations and in more medial planes (data not shown).

NEKL-3 strains tagged with either mKate2 or NeonGreen displayed a pattern of expression similar to that of MLT-3, although both MLT-3 and NEKL-3 had somewhat variable patterns of expression between specimens. NEKL-3 was generally dispersed throughout the hyp7 cytosol and was present in variable-sized puncta (Figure 7B). NEKL-3::NeonGreen puncta strongly overlapped with MLT-3::mKate2 expression in many animals, although in some specimens there were

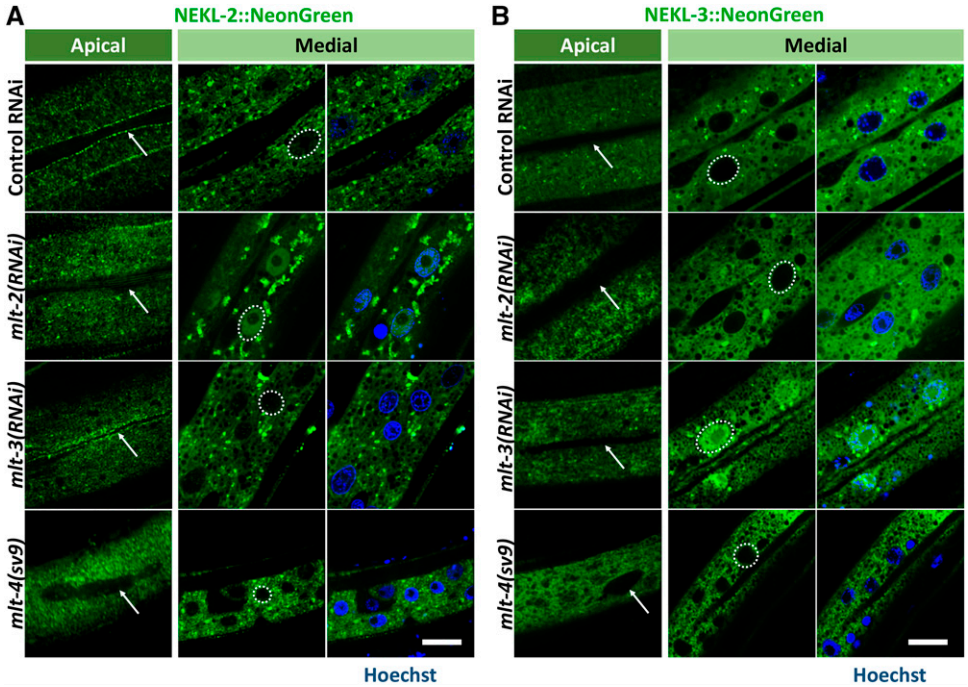

Figure 8 Control of NEKL localization by MLTs. (A, B) Confocal images of NEKL-2::NeonGreen (A) and NEKL-3::NeonGreen (B) in strains treated with control *gfp(RNAi)*, *mlt-2(RNAi)*, or *mlt-3(RNAi)* and in the *mlt-4(sv9)* background. Shown are apical and medial planes of hyp7. DNA was stained with Hoechst (blue) and representative nuclei are outlined by a white dashed line. White arrows indicate the hyp7–seam cell boundary. Because *mlt-4(sv9)* homozygotes arrest at an earlier stage than animals treated with *mlt-2(RNAi)* or *mlt-3(RNAi)* (data not shown), they appear smaller in the panels. Bars, 5 μm.

more NEKL-3::NeonGreen puncta than MLT-3::mKate2 puncta (Figure 7B and data not shown). In contrast, NEKL-3 and MLT-4 did not show strong colocalization, consistent with the weak overlap between MLT-3 and MLT-4 (Figure 4B and Figure 7B). However, NEKL-3 puncta were observed in some animals near the hyp7–seam cell boundary and showed partial colocalization with MLT-4 in this region (Figure 7B). Likewise, NEKL-2 and NEKL-3 did not generally colocalize, consistent with our previous results using multicopy reporters (Yochem *et al.* 2015). Nevertheless, we did observe occasional overlap of NEKL-2 and NEKL-3 at the hyp7–seam cell boundary and, in some animals, we observed moderate-to-extensive colocalization of puncta in other regions of hyp7 (Figure S6 and data not shown).

As was observed for the MLTs, both NEKL-2 and NEKL-3 puncta were highly dynamic and included movement of both large and small particles (data not shown). The mobile nature of both MLT and NEKL puncta may in part account for the variability we observed in their degree of colocalization as well as in their overall expression patterns. Taken together, our expression data provide evidence for stable functional units or complexes comprised of NEKL-2–MLT-2–MLT-4 and NEKL-3–MLT-3, although additional interactions may also occur.

Regulation of NEKL localization by MLT proteins

Based on the above data and the known functions of ankyrin repeat proteins, we hypothesized that MLT proteins may act as molecular scaffolds for NEKL kinases and may control their subcellular localization. To test this we individually depleted *mlt-2*, *mlt-3*, and *mlt-4* in NEKL-2::NeonGreen and NEKL-3::NeonGreen strains using RNAi or mutations and assayed for changes in localization. In the case of NEKL-2 expression, inhibition of *mlt-2* by RNAi prevented normal accumulation at the hyp7–seam cell boundary in most animals (Figure 8A). Furthermore, *mlt-2(RNAi)* led to the accumulation of NEKL-2::NeonGreen in nuclei, which was, in some animals, stronger than the expression in the surrounding cytosol. This was not observed in wild-type animals, although NEKL-2::NeonGreen frequently was expressed at low-to-moderate levels in epidermal nuclei as animals got older (data not shown). Similar to the effect of *mlt-2(RNAi)*, NEKL-2 accumulation was strongly reduced at the hyp7–seam cell boundary in *mlt-4(sv9)* mutants (Figure 8A). Unlike *mlt-2*, however, loss of *mlt-4* activity did not lead to nuclear accumulation of NEKL-2 (Figure 8A). In contrast, we failed to observe corresponding changes in the localization patterns of MLT-2 or MLT-4 after inhibition of *nekl-2* by RNAi (data not shown). Moreover, *mlt-3(RNAi)* did not perturb NEKL-2 localization at the seam cell boundary or affect its exclusion from nuclei, indicating distinct roles for the MLT proteins in their interactions with NEKL kinases (Figure 8A). A role for MLT-2 and MLT-4 in regulating NEKL-2 is consistent with the extensive colocalization of these proteins (Figure 4B and Figure 7A).

In contrast to NEKL-2, NEKL-3 localization was strongly altered following *mlt-3(RNAi)* treatment but did not show dependence on either *mlt-2* or *mlt-4* activities (Figure 8B). Specifically, NEKL-3::NeonGreen became highly enriched in the nuclei of hyp7 after *mlt-3* depletion, an effect that was also observed for NEKL-3::mKate2 (Figure 8B and data not shown). In reciprocal experiments, we failed to observe changes in MLT-3::mKate2 localization following *nekl-3(RNAi)*, suggesting that cytosolic MLT-3 specifically prevents NEKL-3 from entering the nucleus. To further test this model, we carried out a yeast two-hybrid analysis. NEKL-3 bound MLT-3 in both bait and prey configurations (Figure S7),

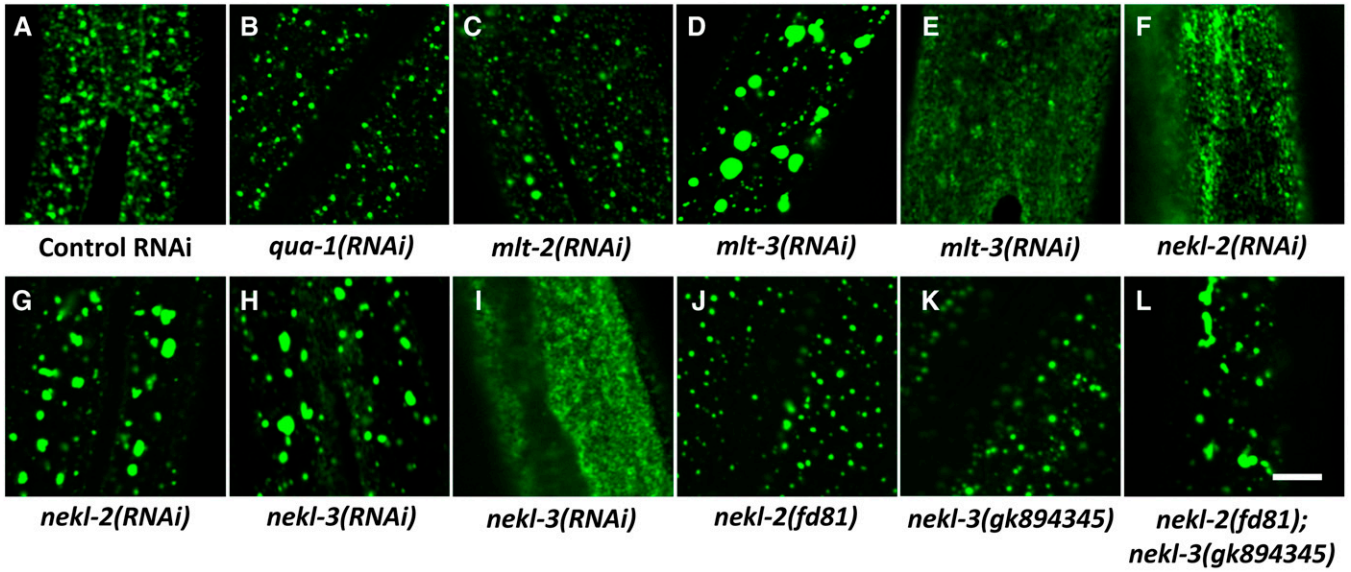

Figure 9 MLT and NEKL proteins control clathrin-mediated endocytosis. (A–L) Confocal images of GFP::CHC-1 apical epidermal expression. Normal punctate expression of GFP::CHC-1 (A) was not perturbed in *qua-1(RNAi)* animals (B), which showed penetrant molting defects. Whereas both *mlt-2(RNAi)* (C) and *mlt-3(RNAi)* (D, E) caused penetrant molting defects, *mlt-3* depletion led to more severe alterations in GFP::CHC-1 expression, which varied from large accumulations (D) to diffuse expression at the apical surface (E). Abnormal accumulations and diffuse expression of GFP::CHC-1 were also observed in some *nekl-2(RNAi)* (F, G) and *nekl-3(RNAi)* (H, I) animals. Whereas hypomorphic alleles of *nekl-2* (*fd81*) and *nekl-3* (*gk894345*) did not perturb GFP::CHC-1 localization (J, K), *nekl-2*(*fd81*); *nekl-3*(*gk894345*) double mutants displayed extensive accumulation of the GFP signal (L). Bar, 5 μm

indicating that this functional interaction might be direct and is consistent with the colocalization data for NEKL-3 and MLT-3 (Figure 7B). Taken together, our findings indicate that ankyrin repeat proteins interact with specific NEKL kinase partners to control their subcellular localization.

Inhibition of the NEKL–MLT network affects intracellular trafficking

Inhibition of *nekl-2* function leads to defects in intracellular trafficking in the epidermis (Yochem *et al.* 2015). Based on our results linking MLT proteins to NEKL-2 and NEKL-3 functions, we postulated that the MLTs may also affect intracellular trafficking during development. To test this we used a strain expressing an integrated fluorescently labeled clathrin heavy chain marker (GFP::CHC-1). This marker allows for the visualization of early events in endocytosis by labeling clathrin-coated pits and early endosomes. In control RNAi-treated animals, GFP::CHC-1 formed small, well-distributed puncta near the apical surface of hyp7 (Figure 9A). As an additional control, we examined GFP::CHC-1 expression in *qua-1(RNAi)* animals, which have penetrant molting defects but do not have perturbed intracellular trafficking (Yochem *et al.* 2015). As anticipated, GFP::CHC-1 appeared similar between control and *qua-1(RNAi)*-treated animals (Figure 9B).

RNAi of *mlt-2* led to a slight increase in the size of GFP::CHC-1 puncta but did not lead to gross changes in subcellular localization (Figure 9C). In contrast, *mlt-3(RNAi)* led to the formation of large and somewhat more basal accumulations of GFP::CHC-1 in a notable proportion of treated animals (Figure 9D). In some other animals, *mlt-3(RNAi)* led to diffuse expression of GFP::CHC-1 near the apical surface (Figure 9E). These variable defects in GFP::CHC-1 localization were also observed following *nekl-2(RNAi)*, which led to both large accumulations and diffuse expression of the marker (Figure 9, F and G). We also observed partially penetrant mislocalization of GFP::CHC-1 following *nekl-3(RNAi)*, as evidenced by either the enhanced-accumulation or diffuse-expression phenotypes (Figure 9, H and I). We further examined the roles of *nekl-2* and *nekl-3* in trafficking using the recently obtained weak hypomorphic alleles. Whereas *nekl-2(fd81)* and *nekl-3(gk894345)* single mutants showed normal GFP::CHC-1 localization, *nekl-2(fd81)*; *nekl-3(gk894345)* double mutants displayed a highly penetrant accumulation phenotype (Figure 9, J–L), further supporting the conclusion that both NEKL-2 and NEKL-3 contribute to endocytic processes.

Discussion

We have identified functions for the conserved ankyrin repeat proteins MLT-2/ANKS6, MLT-3/ANKS3, and MLT-4/INVS in the process of *C. elegans* molting. In addition, we have shown that the MLTs, together with NEKL-2 and NEKL-3, comprise a functional network that affects intracellular trafficking within the major epidermal syncytium, hyp7. Furthermore, NEKL–MLT expression and colocalization data, along with the observation that MLT proteins affect NEKL localization, point to the existence of two distinct functional units comprised of NEKL-2–MLT-2–MLT-4 and NEKL-3–MLT-3. Figure 10 summarizes the major findings from our expression studies. In wild-type animals, NEKL-2, MLT-2, and MLT-4 are coexpressed in puncta throughout the apical surface of hyp7 and show pronounced accumulation at the boundary

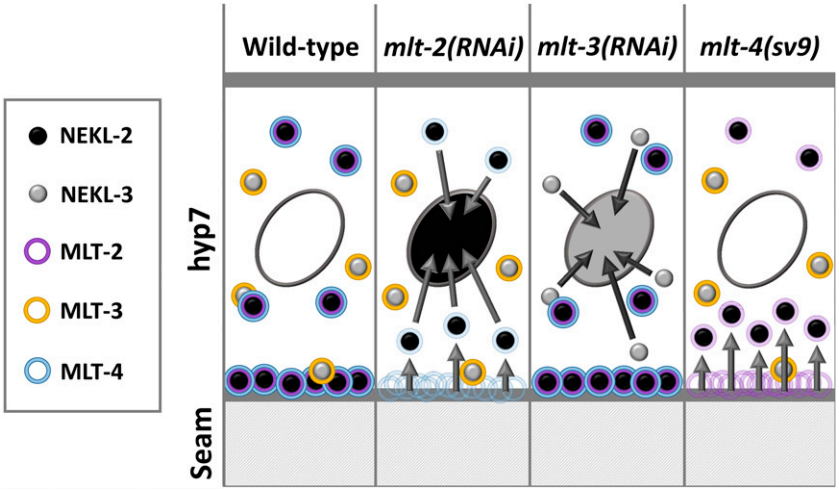

Figure 10 Summary model of MLT and NEKL proteins. Nuclei are indicated by ovals within hyp7. Arrows indicate changes in the subcellular localization of punctae. See *Discussion* for further details.

with the epidermal seam cell. NEKL-3 and MLT-3 also colocalize to epidermal puncta, but these are largely distinct from NEKL-2–MLT-2–MLT-4 puncta and are not highly enriched at the hyp7–seam cell boundary. Nevertheless, occasional overlap of puncta can occur for all the examined members of the NEKL–MLT network and the extent of colocalization can be variable between animals. Furthermore, none of the MLTs and NEKLs is highly expressed in hyp7 nuclei.

Consistent with colocalization data, loss of *mlt-2* or *mlt-4* activity leads to decreased levels of NEKL-2 at the hyp7–seam cell boundary (Figure 10). In addition, loss of *mlt-2*, but not *mlt-4*, results in variable levels of NEKL-2 accumulation within nuclei (Figure 10). Correspondingly, abnormal NEKL-3 nuclear accumulation occurs following the loss of *mlt-3*. In contrast, loss of *mlt-2* or *mlt-4* does not strongly affect NEKL-3 localization, and loss of *mlt-3* does not affect NEKL-2 localization. We also note that we have observed some decreased localization of MLT-4 at the hyp7–seam cell boundary following depletion of *mlt-2*, suggesting that MLT-2 may help to stabilize a NEKL-2–MLT-2–MLT-4 complex (data not shown). Our collective findings are in accordance with our model that the NEKL–MLT protein network contains two largely distinct functional units comprised of NEKL-2–MLT-2–MLT-4 and NEKL-3–MLT-3 and demonstrate that MLT proteins control the subcellular localization of NEKL proteins. Notably, our genetic data do not indicate that members of these two functional units represent two parallel pathways. Rather, data from our enhancement studies suggest that MLTs and NEKLs are more likely part of a single extended network that controls molting (Figure 6).

Importantly, the NEKL–MLT network uncovered by our analysis is likely to be largely conserved in mammals. For example, the MLT-2 ortholog, ANKS6, physically associates both NEK8/NEKL-2 and INVS/MLT-4, although it is unknown if this interaction is direct or indirect (Hoff *et al.* 2013; Czarnecki *et al.* 2015). Our *in vivo* functional data support these findings and further show that NEKL-2 subcellular localization is dependent on both MLT-2 and MLT-4. However, whereas in mammalian cells ANKS6 localization to cilia is dependent on the presence of NEK8 (Czarnecki *et al.* 2015), we did not observe changes in the localization of MLT-2 following NEKL-2 depletion (data not shown). In addition, ANKS6/MLT-2 colocalizes with ANKS3/MLT-3 in kidney cells (Delestre *et al.* 2015), and these proteins physically interact through their SAM domains (Leettola *et al.* 2014). However, because MLT-2 does not contain a predicted SAM domain, this interaction may not be conserved in *C. elegans*, consistent with our observation that MLT-2 and MLT-3 do not extensively colocalize. It was also recently shown that ANKS3/MLT-3 and NEK7/NEKL-3 can be coprecipitated from cell lysates and that ANKS3 is important for the proper localization of NEK7 (Ramachandran *et al.* 2015). This finding is consistent with our expression studies in *C. elegans* and is further supported by our data from yeast two-hybrid studies demonstrating that these proteins likely directly bind to each other.

Our studies also provide new insights into the underlying molecular and cellular functions of the NEKL kinases and their ankyrin repeat partners, which are not well understood. In mammals, mutations affecting NEK8/NEKL-2, ANKS6/MLT-2, INVS/MLT-4, and ANKS3/MLT-3 have been directly linked to a class of diseases termed ciliopathies, which result from defects in the formation of primary cilia (Quarmby and Mahjoub 2005; Otto *et al.* 2008, 2011; Trapp *et al.* 2008; Halbritter *et al.* 2013; Hoff *et al.* 2013; Delestre *et al.* 2015). These include kidney disorders, such as nephronophthisis type 2 (Otto *et al.* 2003) and juvenile cystic kidney disease (Liu *et al.* 2002), as well as situs inversus, cardiovascular abnormalities, liver fibrosis, and defects in other organ systems (Frank *et al.* 2013; Hoff *et al.* 2013; Manning *et al.* 2013). These findings, as well as the expression of NEK8, INVS, ANKS6, and ANKS3 in the proximal ciliary compartment (Shiba *et al.* 2009, 2010; Hoff *et al.* 2013; Delestre *et al.* 2015), have led to the view that these proteins function primarily to control cilia formation. Our findings, however, suggest that ciliogenesis itself may not be the key central function of these proteins. Specifically, members of the *C. elegans* NEKL–MLT network play a critical role in an

epidermal tissue that does not contain primary cilia, implying a more general cellular function. Consistent with this, mammalian NEK8 is detected in puncta throughout the cytoplasm, and only a minor fraction of NEK8 localizes to ciliary structures (Holland *et al.* 2002; Liu *et al.* 2002; Trapp *et al.* 2008; Shiba *et al.* 2010; Fukui *et al.* 2012; McCooke *et al.* 2012). In addition, INVS/MLT-4 regulates cortical actin during cell division (Werner *et al.* 2013), and NEK8 may affect gross actin levels as well as actin organization (Liu *et al.* 2002; Bowers and Boylan 2004).

In the case of the mammalian NEKL-3 orthologs, NEK6 and NEK7, the majority of studies have focused on the role of these kinases in the cell division process including centrosome separation (Sdelci *et al.* 2011), spindle formation, and cytokinesis (O'Regan *et al.* 2007; O'Regan and Fry 2009). These functions also link well to the reported involvement of NEK6 and NEK7 in tumorigenesis (Nassirpour *et al.* 2010; Wang *et al.* 2013; Zhou *et al.* 2016). Interestingly, we have not detected functions for NEKL-3, or any other component of the NEKL–MLT network, in cell division processes in *C. elegans* (Yochem *et al.* 2015). Although this could reflect divergent functions for these closely related orthologs between species, we have shown that *nekl-3(sv3)* mutants can be rescued by expression of mammalian NEK6 and NEK7 (data not shown). This finding, along with the high degree of sequence conservation among these proteins, suggests a more fundamental function for the NEKL-3/NEK6/NEK7 orthologs that may have been previously overlooked. Furthermore, the relative importance of mammalian NEK6 and NEK7 in mitosis is not fully resolved. Knockout of *NEK6* in mice leads to no reported cell division defects (Bian *et al.* 2014), and *NEK7*$^{-/-}$ neonates are initially viable and display relatively minimal defects in cell division (Salem *et al.* 2010). Moreover, several observations suggest that NEK6 and NEK7 may also be associated with non-cell-cycle functions. For example, NEK6 and NEK7 are expressed at high levels in the cytoplasm during interphase (Kim *et al.* 2007; O'Regan and Fry 2009; de Souza *et al.* 2014), and NEK7 affects microtubule dynamics during interphase (Kang *et al.* 2013). In addition, most NEK6 and NEK7 interactors identified by proteomics are not linked specifically to cell cycle functions and include proteins associated with the cytoskeleton (*e.g.*, TUBB, actin, CDC42, MAP7D1, MAP2, CLASP1, and CLASP2) and vesicular trafficking (*e.g.*, CDC42, SNX26, RBLE1, ATP6V1G1, AP2A, AP2B, and RAB32) (Meirelles *et al.* 2011, 2014; de Souza *et al.* 2014).

Intriguingly, several studies have suggested possible functions for NIMA family kinases in intracellular trafficking. In one case, a high-throughput siRNA screen of 590 human kinases by Pelkmans *et al.* (2005) identified 208 candidate regulators of endocytosis including NEK6, NEK7, and NEK8. In addition, studies in nonmetazoan species have implicated members of the NIMA kinase family in a variety of functions unrelated to the cell cycle or ciliogenesis. For example, three *Arabidopsis thaliana* NEKs (related to NEKL-2) have been implicated in epidermal root tip growth through the possible regulation of microtubules (Sakai *et al.* 2008; Motose *et al.* 2011, 2012). Perhaps most notable was the recent report that *Aspergillus nidulans* nimA, which was originally identified for its role in mitosis, also controls polarized cell growth and localizes to microtubule plus ends in an EB1-dependent manner during interphase (Govindaraghavan *et al.* 2014). This study also showed that mutations in both the *A. nidulans* and *Saccharomyces cerevisiae* NIMA orthologs (*nimA* and *kin3*) are synthetically lethal with mutations in genes encoding ESCRT complex components, which promote membrane remodeling and endosome maturation (McCullough *et al.* 2013; Govindaraghavan *et al.* 2014). Although the functional connection between nimA and ESCRT proteins is unknown, this finding implicates NIMA kinases in processes linked to intracellular trafficking. Collectively, these studies, together with our own findings, support the model that at least some of the underlying conserved functions of NIMA family members are unrelated to cell cycle control or ciliogenesis and may encompass functions associated with vesicle trafficking and the interphase cytoskeleton.

Our observation that inhibition of MLT and NEKL proteins leads to defects in clathrin-dependent endocytosis in hyp7 raises the possibility that regulation of intracellular trafficking may be a key function of the NEKL–MLT network. In support of this model, we previously showed that NEKL-2 affects the expression of several endosomal markers including GFP::EEA-1, GFP::RAB-5, GFP::SNX-1, and GFP::CHC-1 (Yochem *et al.* 2015) and in the current study have further implicated NEKL-3, MLT-3, and, to a lesser extent, MLT-2 in controlling clathrin-dependent endocytosis. Interestingly, MLT-3 contains an FXDXF motif, which has been associated with accessory protein recruitment in clathrin-mediated endocytosis (Brett *et al.* 2002), although this motif is not conserved in human ANKS3. We also previously reported that NEKL-2 affects the localization of LRP-1/megalin, a member of the low-density lipoprotein receptor family (Yochem *et al.* 2015). LRP-1 is required for normal molting and is thought to function in the process of cholesterol uptake by the epidermis (Yochem *et al.* 1999; May *et al.* 2007). Consistent with this, cholesterol is essential for molting in *C. elegans* (Yochem *et al.* 1999; Merris *et al.* 2003; Entchev and Kurzchalia 2005; Roudier *et al.* 2005). In addition, studies on mammalian megalin suggest that *C. elegans* LRP-1 could promote molting in part by regulating the uptake of proteases and protease inhibitors (May *et al.* 2007; Marzolo and Farfan 2011; Etique *et al.* 2013). In addition to LRP-1, several other genes required for molting also affect intracellular trafficking and sterol–LRP-1 uptake including *dab-1/Disabled*, *hgrs-1/VPS27*, and *sec-23/SEC23* (Kamikura and Cooper 2003; Roberts *et al.* 2003; Roudier *et al.* 2005; Holmes *et al.* 2007; Yochem *et al.* 2015).

The regulation of intracellular trafficking may not, however, be a primary or direct function of the NEKL–MLT network, and perturbation of trafficking may not be the main cause of molting defects in *nekl* and *mlt* mutants. Notably, the observed effects on endocytosis markers following inhibition of either the *mlt* or *nekl genes* are quite variable and incompletely penetrant, even in cases where the induced molting defects are fully penetrant. Moreover, we have not observed a clear correlation between the

severity of molting defects (in individual animals or populations) and the extent of changes in the expression pattern of endosomal marker GFP::CHC-1. Thus, it seems likely that MLT and NEKL proteins control cellular processes that affect intracellular trafficking but are not absolutely required for this function.

Based on our current data, we suggest that defects in intracellular trafficking in *nekl* and *mlt* mutants may influence molting but that other cellular functions controlled by these genes are likely to further impact this process. For example, the NEKL–MLT network could affect the actin cytoskeleton, which is required for the formation of clathrin-coated vesicles as well as other fundamental functions and properties of cells (Qualmann *et al.* 2000; Smythe and Ayscough 2006; Mooren *et al.* 2012). Alternatively, the NEKL–MLT pathway could regulate interphase microtubules, which are also critical for vesicular trafficking, as well as cell polarity and organization (Soldati and Schliwa 2006; Siegrist and Doe 2007; Zhang *et al.* 2014). We note that the subcellular localization and dynamic nature of both NEKL and MLT puncta could be consistent with a variety of functions including intracellular trafficking and/or the regulation of cytoskeletal components. Future studies in *C. elegans*, including the further characterization of the NEKL–MLT subcellular compartments and the identification of NEKL target substrates, will greatly help to resolve questions regarding the conserved molecular functions of the NEKL–MLT network. In addition, these studies should shed light on our understanding of the widespread pathological conditions that arise from mutations in members of the NEKL–MLT network.

Acknowledgments

We foremost acknowledge the scientific input, generosity, and expertise of John Yochem, who started the molting project in the Fay Lab. We are also indebted to Bob Herman, Lihsia Chen, and Simon Tuck for their support of this project; to Amy Fluet for editing; to Jay Gatlin for microscopy support; to Barth Grant for providing strains and scientific input; and to Leslie Bell, Evguenia Karina, Daniel Dickinson, and Bob Goldstein for additional support. Some strains used in these studies were provided by the Caenorhabditis Genetics Center, which is funded by the United States National Institutes of Health (NIH) Office of Research Infrastructure Programs (P40 OD010440), and National BioResource Project, Tokyo (The *C. elegans* Deletion Mutant Consortium 2012). Cosmid clones were provided by the Wellcome Trust, UK. Support at the University of Wyoming was from the NIH grant GM-066868 to D.S.F.

Literature Cited

Abascal, F., R. Zardoya, and D. Posada, 2005 ProtTest: selection of best-fit models of protein evolution. Bioinformatics 21: 2104–2105.

Ahringer, J., 2005 Reverse genetics (April 6, 2006), *WormBook*, ed. The *C. elegans* Research Community WormBook, doi/10.1895/wormbook.1.47.1, http://www.wormbook.org.

Altincicek, B., M. Fischer, K. Luersen, M. Boll, U. Wenzel *et al.*, 2010 Role of matrix metalloproteinase ZMP-2 in pathogen resistance and development in *Caenorhabditis elegans*. Dev. Comp. Immunol. 34: 1160–1169.

Arribere, J. A., R. T. Bell, B. X. Fu, K. L. Artiles, P. S. Hartman *et al.*, 2014 Efficient marker-free recovery of custom genetic modifications with CRISPR/Cas9 in *Caenorhabditis elegans*. Genetics 198: 837–846.

Bian, Z., H. Liao, Y. Zhang, Q. Wu, H. Zhou *et al.*, 2014 Never in mitosis gene A related kinase-6 attenuates pressure overload-induced activation of the protein kinase B pathway and cardiac hypertrophy. PLoS One 9: e96095.

Bowers, A. J., and J. F. Boylan, 2004 Nek8, a NIMA family kinase member, is overexpressed in primary human breast tumors. Gene 328: 135–142.

Brenner, S., 1974 The genetics of *Caenorhabditis elegans*. Genetics 77: 71–94.

Brett, T. J., L. M. Traub, and D. H. Fremont, 2002 Accessory protein recruitment motifs in clathrin-mediated endocytosis. Structure 10: 797–809.

Chisholm, A. D., and S. Xu, 2012 The *Caenorhabditis elegans* epidermis as a model skin. II: differentiation and physiological roles. Wiley Interdiscip. Rev. Dev. Biol. 1: 879–902.

Cox, T. R., and J. T. Erler, 2011 Remodeling and homeostasis of the extracellular matrix: implications for fibrotic diseases and cancer. Dis. Model. Mech. 4: 165–178.

Crooks, G. E., G. Hon, J. M. Chandonia, and S. E. Brenner, 2004 WebLogo: a sequence logo generator. Genome Res. 14: 1188–1190.

Czarnecki, P. G., G. C. Gabriel, D. K. Manning, M. Sergeev, K. Lemke *et al.*, 2015 ANKS6 is the critical activator of NEK8 kinase in embryonic situs determination and organ patterning. Nat. Commun. 6: 6023.

Davis, M. W., A. J. Birnie, A. C. Chan, A. P. Page, and E. M. Jorgensen, 2004 A conserved metalloprotease mediates ecdysis in *Caenorhabditis elegans*. Development 131: 6001–6008.

Delestre, L., Z. Bakey, C. Prado, S. Hoffmann, M. T. Bihoreau *et al.*, 2015 ANKS3 co-localises with ANKS6 in mouse renal cilia and is associated with vasopressin signaling and apoptosis *in vivo* in mice. PLoS One 10: e0136781.

de Souza, E. E., G. V. Meirelles, B. B. Godoy, A. M. Perez, J. H. Smetana *et al.*, 2014 Characterization of the human NEK7 interactome suggests catalytic and regulatory properties distinct from those of NEK6. J. Proteome Res. 13: 4074–4090.

Dickinson, D. J., A. M. Pani, J. K. Heppert, C. D. Higgins, and B. Goldstein, 2015 Streamlined genome engineering with a self-excising drug selection cassette. Genetics 200: 1035–1049.

Dinkel, H., K. Van Roey, S. Michael, M. Kumar, B. Uyar *et al.*, 2016 ELM 2016—data update and new functionality of the eukaryotic linear motif resource. Nucleic Acids Res. 44: D294–D300.

Entchev, E. V., and T. V. Kurzchalia, 2005 Requirement of sterols in the life cycle of the nematode *Caenorhabditis elegans*. Semin. Cell Dev. Biol. 16: 175–182.

Etique, N., L. Verzeaux, S. Dedieu, and H. Emonard, 2013 LRP-1: a checkpoint for the extracellular matrix proteolysis. BioMed Res. Int. 2013: 152163.

Frand, A. R., S. Russel, and G. Ruvkun, 2005 Functional genomic analysis of *C. elegans* molting. PLoS Biol. 3: e312.

Frank, V., S. Habbig, M. P. Bartram, T. Eisenberger, H. E. Veenstra-Knol *et al.*, 2013 Mutations in NEK8 link multiple organ dysplasia with altered Hippo signalling and increased c-MYC expression. Hum. Mol. Genet. 22: 2177–2185.

Fukui, H., D. Shiba, K. Asakawa, K. Kawakami, and T. Yokoyama, 2012 The ciliary protein Nek8/Nphp9 acts downstream of Inv/Nphp2 during pronephros morphogenesis and left-right establishment in zebrafish. FEBS Lett. 586: 2273–2279.

Gissendanner, C. R., and A. E. Sluder, 2000 *nhr-25*, the *Caenorhabditis elegans* ortholog of *ftz-f1*, is required for epidermal and somatic gonad development. Dev. Biol. 221: 259–272.

Gooyit, M., N. Tricoche, S. Javor, S. Lustigman, and K. D. Janda, 2015 Exploiting the polypharmacology of β-carbolines to disrupt *O. volvulus* molting. ACS Med. Chem. Lett. 6: 339–343.

Govindaraghavan, M., S. L. McGuire Anglin, K. F. Shen, N. Shukla, C. P. De Souza *et al.*, 2014 Identification of interphase functions for the NIMA kinase involving microtubules and the ESCRT pathway. PLoS Genet. 10: e1004248.

Halbritter, J., J. D. Porath, K. A. Diaz, D. A. Braun, S. Kohl *et al.*, 2013 Identification of 99 novel mutations in a worldwide cohort of 1,056 patients with a nephronophthisis-related ciliopathy. Hum. Genet. 132: 865–884.

Hao, L., K. Mukherjee, S. Liegeois, D. Baillie, M. Labouesse *et al.*, 2006 The *hedgehog*-related gene *qua*-1 is required for molting in *Caenorhabditis elegans*. Dev. Dyn. 235: 1469–1481.

Hashmi, S., J. Zhang, Y. Oksov, and S. Lustigman, 2004 The *Caenorhabditis elegans* cathepsin Z-like cysteine protease, *Ce*-CPZ-1, has a multifunctional role during the worms' development. J. Biol. Chem. 279: 6035–6045.

Hayes, G. D., A. R. Frand, and G. Ruvkun, 2006 The *mir-84* and *let-7* paralogous microRNA genes of *Caenorhabditis elegans* direct the cessation of molting via the conserved nuclear hormone receptors NHR-23 and NHR-25. Development 133: 4631–4641.

Hirsh, D., D. Oppenheim, and M. Klass, 1976 Development of the reproductive system of *Caenorhabditis elegans*. Dev. Biol. 49: 200–219.

Hoff, S., J. Halbritter, D. Epting, V. Frank, T. M. Nguyen *et al.*, 2013 ANKS6 is a central component of a nephronophthisis module linking NEK8 to INVS and NPHP3. Nat. Genet. 45: 951–956.

Holland, P. M., A. Milne, K. Garka, R. S. Johnson, C. Willis *et al.*, 2002 Purification, cloning, and characterization of Nek8, a novel NIMA-related kinase, and its candidate substrate Bicd2. J. Biol. Chem. 277: 16229–16240.

Hollenbeck, J. J., D. J. Danner, R. M. Landgren, T. K. Rainbolt, and D. S. Roberts, 2012 Designed ankyrin repeat proteins as scaffolds for multivalent recognition. Biomacromolecules 13: 1996–2002.

Holmes, A., A. Flett, D. Coudreuse, H. C. Korswagen, and J. Pettitt, 2007 *C. elegans* disabled is required for cell-type specific endocytosis and is essential in animals lacking the AP-3 adaptor complex. J. Cell Sci. 120: 2741–2751.

Jia, K., P. S. Albert, and D. L. Riddle, 2002 DAF-9, a cytochrome P450 regulating *C. elegans* larval development and adult longevity. Development 129: 221–231.

Kamikura, D. M., and J. A. Cooper, 2003 Lipoprotein receptors and a disabled family cytoplasmic adaptor protein regulate EGL-17/FGF export in *C. elegans*. Genes Dev. 17: 2798–2811.

Kang, Y. L., J. Yochem, L. Bell, E. B. Sorensen, L. Chen *et al.*, 2013 *Caenorhabditis elegans* reveals a FxNPxY-independent low-density lipoprotein receptor internalization mechanism mediated by epsin1. Mol. Biol. Cell 24: 308–318.

Katoh, K., and D. M. Standley, 2013 MAFFT multiple sequence alignment software version 7: improvements in performance and usability. Mol. Biol. Evol. 30: 772–780.

Kim, C. A., and J. U. Bowie, 2003 SAM domains: uniform structure, diversity of function. Trends Biochem. Sci. 28: 625–628.

Kim, T. H., Y. J. Kim, J. W. Cho, and J. Shim, 2011 A novel zinc-carboxypeptidase SURO-1 regulates cuticle formation and body morphogenesis in *Caenorhabditis elegans*. FEBS Lett. 585: 121–127.

Kim, Y., M. S. Gentry, T. E. Harris, S. E. Wiley, J. C. Lawrence, Jr. *et al.*, 2007 A conserved phosphatase cascade that regulates nuclear membrane biogenesis. Proc. Natl. Acad. Sci. USA 104: 6596–6601.

Kostrouchova, M., M. Krause, Z. Kostrouch, and J. E. Rall, 1998 CHR3: a Caenorhabditis elegans orphan nuclear hormone receptor required for proper epidermal development and molting. Development 125: 1617–1626.

Kostrouchova, M., M. Krause, Z. Kostrouch, and J. E. Rall, 2001 Nuclear hormone receptor CHR3 is a critical regulator of all four larval molts of the nematode *Caenorhabditis elegans*. Proc. Natl. Acad. Sci. USA 98: 7360–7365.

Kouns, N. A., J. Nakielna, F. Behensky, M. W. Krause, Z. Kostrouch *et al.*, 2011 NHR-23 dependent collagen and hedgehog-related genes required for molting. Biochem. Biophys. Res. Commun. 413: 515–520.

Kuervers, L. M., C. L. Jones, N. J. O'Neil, and D. L. Baillie, 2003 The sterol modifying enzyme LET-767 is essential for growth, reproduction and development in *Caenorhabditis elegans*. Mol. Genet. Genomics 270: 121–131.

Leettola, C. N., M. J. Knight, D. Cascio, S. Hoffman, and J. U. Bowie, 2014 Characterization of the SAM domain of the PKD-related protein ANKS6 and its interaction with ANKS3. BMC Struct. Biol. 14: 17.

Letunic, I., and P. Bork, 2016 Interactive tree of life (iTOL) v3: an online tool for the display and annotation of phylogenetic and other trees. Nucleic Acids Res. 44: W242–W245.

Letunic, I., T. Doerks, and P. Bork, 2015 SMART: recent updates, new developments and status in 2015. Nucleic Acids Res. 43: D257–D260.

Li, W., A. Cowley, M. Uludag, T. Gur, H. McWilliam *et al.*, 2015 The EMBL-EBI bioinformatics web and programmatic tools framework. Nucleic Acids Res. 43: W580–W584.

Li, Y., and Y. K. Paik, 2011 A potential role for fatty acid biosynthesis genes during molting and cuticle formation in Caenorhabditis elegans. BMB Rep. 44: 285–290.

Liu, S., W. Lu, T. Obara, S. Kuida, J. Lehoczky *et al.*, 2002 A defect in a novel Nek-family kinase causes cystic kidney disease in the mouse and in zebrafish. Development 129: 5839–5846.

Mahjoub, M. R., M. L. Trapp, and L. M. Quarmby, 2005 NIMA-related kinases defective in murine models of polycystic kidney diseases localize to primary cilia and centrosomes. J. Am. Soc. Nephrol. 16: 3485–3489.

Manning, D. K., M. Sergeev, R. G. van Heesbeen, M. D. Wong, J. H. Oh *et al.*, 2013 Loss of the ciliary kinase Nek8 causes left-right asymmetry defects. J. Am. Soc. Nephrol. 24: 100–112.

Marzolo, M. P., and P. Farfan, 2011 New insights into the roles of megalin/LRP2 and the regulation of its functional expression. Biol. Res. 44: 89–105.

May, P., E. Woldt, R. L. Matz, and P. Boucher, 2007 The LDL receptor-related protein (LRP) family: an old family of proteins with new physiological functions. Ann. Med. 39: 219–228.

McCooke, J. K., R. Appels, R. A. Barrero, A. Ding, J. E. Ozimek-Kulik *et al.*, 2012 A novel mutation causing nephronophthisis in the Lewis polycystic kidney rat localises to a conserved RCC1 domain in Nek8. BMC Genomics 13: 393.

McCullough, J., L. A. Colf, and W. I. Sundquist, 2013 Membrane fission reactions of the mammalian ESCRT pathway. Annu. Rev. Biochem. 82: 663–692.

McWilliam, H., W. Li, M. Uludag, S. Squizzato, Y. M. Park *et al.*, 2013 Analysis tool web services from the EMBL-EBI. Nucleic Acids Res. 41: W597–W600.

Meirelles, G. V., J. C. Silva, A. Mendonca Yde, C. H. Ramos, I. L. Torriani *et al.*, 2011 Human Nek6 is a monomeric mostly globular kinase with an unfolded short N-terminal domain. BMC Struct. Biol. 11: 12.

Meirelles, G. V., A. M. Perez, E. E. de Souza, F. L. Basei, P. F. Papa *et al.*, 2014 "Stop Ne(c)king around": how interactomics contributes to functionally characterize Nek family kinases. World J. Biol. Chem. 5: 141–160.

Merris, M., W. G. Wadsworth, U. Khamrai, R. Bittman, D. J. Chitwood *et al.*, 2003 Sterol effects and sites of sterol accumulation in Caenorhabditis elegans: developmental requirement for 4α-methyl sterols. J. Lipid Res. 44: 172–181.

Monsalve, G. C., and A. R. Frand, 2012 Toward a unified model of developmental timing: a "molting" approach. Worm 1: 221–230.

Mooren, O. L., B. J. Galletta, and J. A. Cooper, 2012 Roles for actin assembly in endocytosis. Annu. Rev. Biochem. 81: 661–686.
Mosavi, L. K., T. J. Cammett, D. C. Desrosiers, and Z. Y. Peng, 2004 The ankyrin repeat as molecular architecture for protein recognition. Protein Sci. 13: 1435–1448.
Motose, H., T. Hamada, K. Yoshimoto, T. Murata, M. Hasebe *et al.*, 2011 NIMA-related kinases 6, 4, and 5 interact with each other to regulate microtubule organization during epidermal cell expansion in Arabidopsis thaliana. Plant J. 67: 993–1005.
Motose, H., S. Takatani, T. Ikeda, and T. Takahashi, 2012 NIMA-related kinases regulate directional cell growth and organ development through microtubule function in *Arabidopsis thaliana*. Plant Signal. Behav. 7: 1552–1555.
Murata, K., M. Kudo, F. Onuma, and T. Motoyama, 1984 Changes of collagen types at various stages of human liver cirrhosis. Hepatogastroenterology 31: 158–161.
Nassirpour, R., L. Shao, P. Flanagan, T. Abrams, B. Jallal *et al.*, 2010 Nek6 mediates human cancer cell transformation and is a potential cancer therapeutic target. Mol. Cancer Res. 8: 717–728.
Nielsen, K., J. O. Clemmesen, E. Vassiliadis, and B. Vainer, 2014 Liver collagen in cirrhosis correlates with portal hypertension and liver dysfunction. APMIS 122: 1213–1222.
O'Regan, L., and A. M. Fry, 2009 The Nek6 and Nek7 protein kinases are required for robust mitotic spindle formation and cytokinesis. Mol. Cell. Biol. 29: 3975–3990.
O'Regan, L., J. Blot, and A. M. Fry, 2007 Mitotic regulation by NIMA-related kinases. Cell Div. 2: 25.
Otto, E. A., B. Schermer, T. Obara, J. F. O'Toole, K. S. Hiller *et al.*, 2003 Mutations in INVS encoding inversin cause nephronophthisis type 2, linking renal cystic disease to the function of primary cilia and left-right axis determination. Nat. Genet. 34: 413–420.
Otto, E. A., M. L. Trapp, U. T. Schultheiss, J. Helou, L. M. Quarmby *et al.*, 2008 NEK8 mutations affect ciliary and centrosomal localization and may cause nephronophthisis. J. Am. Soc. Nephrol. 19: 587–592.
Otto, E. A., G. Ramaswami, S. Janssen, M. Chaki, S. J. Allen *et al.*, 2011 Mutation analysis of 18 nephronophthisis associated ciliopathy disease genes using a DNA pooling and next generation sequencing strategy. J. Med. Genet. 48: 105–116.
Page, A. P., and I. L. Johnstone, 2007 The cuticle (March 19, 2007), *WormBook* , ed. The *C. elegans* Research Community WormBook, doi/10.1895/wormbook.1.138.1, http://www.wormbook.org.
Page, A. P., G. Stepek, A. D. Winter, and D. Pertab, 2014 Enzymology of the nematode cuticle: a potential drug target? Int. J. Parasitol. Drugs Drug Resist. 4: 133–141.
Paix, A., Y. Wang, H. E. Smith, C. Y. Lee, D. Calidas *et al.*, 2014 Scalable and versatile genome editing using linear DNAs with microhomology to Cas9 sites in *Caenorhabditis elegans*. Genetics 198: 1347–1356.
Pelkmans, L., E. Fava, H. Grabner, M. Hannus, B. Habermann *et al.*, 2005 Genome-wide analysis of human kinases in clathrin- and caveolae/raft-mediated endocytosis. Nature 436: 78–86.
Pettersen, E. F., T. D. Goddard, C. C. Huang, G. S. Couch, D. M. Greenblatt *et al.*, 2004 UCSF Chimera—a visualization system for exploratory research and analysis. J. Comput. Chem. 25: 1605–1612.
Ponticos, M., I. Papaioannou, S. Xu, A. M. Holmes, K. Khan *et al.*, 2015 Failed degradation of JunB contributes to overproduction of type I collagen and development of dermal fibrosis in patients with systemic sclerosis. Arthritis Rheumatol. 67: 243–253.
Qualmann, B., M. M. Kessels, and R. B. Kelly, 2000 Molecular links between endocytosis and the actin cytoskeleton. J. Cell Biol. 150: F111–F116.
Quarmby, L. M., and M. R. Mahjoub, 2005 Caught Nek-ing: cilia and centrioles. J. Cell Sci. 118: 5161–5169.
Raghu, G., S. Masta, D. Meyers, and A. S. Narayanan, 1989 Collagen synthesis by normal and fibrotic human lung fibroblasts and the effect of transforming growth factor-β. Am. Rev. Respir. Dis. 140: 95–100.
Ramachandran, H., C. Engel, B. Muller, J. Dengjel, G. Walz *et al.*, 2015 Anks3 alters the sub-cellular localization of the Nek7 kinase. Biochem. Biophys. Res. Commun. 464: 901–907.
Rhoads, A. R., and F. Friedberg, 1997 Sequence motifs for calmodulin recognition. FASEB J. 11: 331–340.
Rice, P., I. Longden, and A. Bleasby, 2000 EMBOSS: the European Molecular Biology Open Software Suite. Trends Genet. 16: 276–277.
Roberts, B., C. Clucas, and I. L. Johnstone, 2003 Loss of SEC-23 in *Caenorhabditis elegans* causes defects in oogenesis, morphogenesis, and extracellular matrix secretion. Mol. Biol. Cell 14: 4414–4426.
Roudier, N., C. Lefebvre, and R. Legouis, 2005 CeVPS-27 is an endosomal protein required for the molting and the endocytic trafficking of the low-density lipoprotein receptor-related protein 1 in *Caenorhabditis elegans*. Traffic 6: 695–705.
Roy, A., A. Kucukural, and Y. Zhang, 2010 I-TASSER: a unified platform for automated protein structure and function prediction. Nat. Protoc. 5: 725–738.
Sakai, T., H. Honing, M. Nishioka, Y. Uehara, M. Takahashi *et al.*, 2008 Armadillo repeat-containing kinesins and a NIMA-related kinase are required for epidermal-cell morphogenesis in Arabidopsis. Plant J. 53: 157–171.
Salem, H., I. Rachmin, N. Yissachar, S. Cohen, A. Amiel *et al.*, 2010 Nek7 kinase targeting leads to early mortality, cytokinesis disturbance and polyploidy. Oncogene 29: 4046–4057.
Sdelci, S., M. T. Bertran, and J. Roig, 2011 Nek9, Nek6, Nek7 and the separation of centrosomes. Cell Cycle 10: 3816–3817.
Shaye, D. D., and I. Greenwald, 2011 OrthoList: a compendium of *C. elegans* genes with human orthologs. PLoS One 6: e20085.
Shiba, D., Y. Yamaoka, H. Hagiwara, T. Takamatsu, H. Hamada *et al.*, 2009 Localization of Inv in a distinctive intraciliary compartment requires the C-terminal ninein-homolog-containing region. J. Cell Sci. 122: 44–54.
Shiba, D., D. K. Manning, H. Koga, D. R. Beier, and T. Yokoyama, 2010 Inv acts as a molecular anchor for Nphp3 and Nek8 in the proximal segment of primary cilia. Cytoskeleton (Hoboken) 67: 112–119.
Siegrist, S. E., and C. Q. Doe, 2007 Microtubule-induced cortical cell polarity. Genes Dev. 21: 483–496.
Singh, R. N., and J. E. Sulston, 1978 Some observations on the moulting of Caenorhabditis elegans. Nematologica 24: 63–71.
Smythe, E., and K. R. Ayscough, 2006 Actin regulation in endocytosis. J. Cell Sci. 119: 4589–4598.
Soldati, T., and M. Schliwa, 2006 Powering membrane traffic in endocytosis and recycling. Nat. Rev. Mol. Cell Biol. 7: 897–908.
Specks, U., A. Nerlich, T. V. Colby, I. Wiest, and R. Timpl, 1995 Increased expression of type VI collagen in lung fibrosis. Am. J. Respir. Crit. Care Med. 151: 1956–1964.
Stenvall, J., J. C. Fierro-Gonzalez, P. Swoboda, K. Saamarthy, Q. Cheng *et al.*, 2011 Selenoprotein TRXR-1 and GSR-1 are essential for removal of old cuticle during molting in *Caenorhabditis elegans*. Proc. Natl. Acad. Sci. USA 108: 1064–1069.
Stepek, G., G. McCormack, A. J. Birnie, and A. P. Page, 2011 The astacin metalloprotease moulting enzyme NAS-36 is required for normal cuticle ecdysis in free-living and parasitic nematodes. Parasitology 138: 237–248.
Stiernagle, T., 2006 Maintenance of *C. elegans* (February 11, 2006), *WormBook*, ed. The *C. elegans* Research Community WormBook, doi/10.1895/wormbook.1.101.1, http://www.wormbook.org.

Sulston, J. E., E. Schierenberg, J. G. White, and J. N. Thomson, 1983 The embryonic cell lineage of the nematode *Caenorhabditis elegans*. Dev. Biol. 100: 64–119.

Suzuki, M., N. Sagoh, H. Iwasaki, H. Inoue, and K. Takahashi, 2004 Metalloproteases with EGF, CUB, and thrombospondin-1 domains function in molting of Caenorhabditis elegans. Biol. Chem. 385: 565–568.

The *C. elegans* Deletion Mutant Consortium, 2012 Large-scale screening for targeted knockouts in the *Caenorhabditis elegans* genome. G3 2: 1415–1425.

Thompson, O., M. Edgley, P. Strasbourger, S. Flibotte, B. Ewing *et al.*, 2013 The million mutation project: a new approach to genetics in *Caenorhabditis elegans*. Genome Res. 23: 1749–1762.

Timmons, L., D. L. Court, and A. Fire, 2001 Ingestion of bacterially expressed dsRNAs can produce specific and potent genetic interference in *Caenorhabditis elegans*. Gene 263: 103–112.

Todd, N. W., I. G. Luzina, and S. P. Atamas, 2012 Molecular and cellular mechanisms of pulmonary fibrosis. Fibrogenesis Tissue Repair 5: 11.

Trapp, M. L., A. Galtseva, D. K. Manning, D. R. Beier, N. D. Rosenblum *et al.*, 2008 Defects in ciliary localization of Nek8 is associated with cystogenesis. Pediatr. Nephrol. 23: 377–387.

Voronin, D. A., and E. V. Kiseleva, 2008 Functional role of proteins containing ankyrin repeats. Cell Tiss. Biol. DOI: 10.1134/S1990519X0801001X.

Wang, D., S. Kennedy, D. Conte, Jr., J. K. Kim, H. W. Gabel *et al.*, 2005 Somatic misexpression of germline P granules and enhanced RNA interference in retinoblastoma pathway mutants. Nature 436: 593–597.

Wang, R., Y. Song, X. Xu, Q. Wu, and C. Liu, 2013 The expression of Nek7, FoxM1, and Plk1 in gallbladder cancer and their relationships to clinicopathologic features and survival. Clin. Transl. Oncol. 15: 626–632.

Warburton-Pitt, S. R., A. R. Jauregui, C. Li, J. Wang, M. R. Leroux *et al.*, 2012 Ciliogenesis in *Caenorhabditis elegans* requires genetic interactions between ciliary middle segment localized NPHP-2 (inversin) and transition zone-associated proteins. J. Cell Sci. 125: 2592–2603.

Waterhouse, A. M., J. B. Procter, D. M. Martin, M. Clamp, and G. J. Barton, 2009 Jalview Version 2—a multiple sequence alignment editor and analysis workbench. Bioinformatics 25: 1189–1191.

Wendler, F., X. Franch-Marro, and J. P. Vincent, 2006 How does cholesterol affect the way Hedgehog works? Development 133: 3055–3061.

Werner, M. E., H. H. Ward, C. L. Phillips, C. Miller, V. H. Gattone *et al.*, 2013 Inversin modulates the cortical actin network during mitosis. Am. J. Physiol. Cell Physiol. 305: C36–C47.

Wicks, S. R., R. T. Yeh, W. R. Gish, R. H. Waterston, and R. H. Plasterk, 2001 Rapid gene mapping in *Caenorhabditis elegans* using a high density polymorphism map. Nat. Genet. 28: 160–164.

Yang, J., R. Yan, A. Roy, D. Xu, J. Poisson *et al.*, 2015 The I-TASSER Suite: protein structure and function prediction. Nat. Methods 12: 7–8.

Yochem, J., 2006 Nomarski images for learning the anatomy, with tips for mosaic analysis (January 24, 2006), *WormBook*, ed. The *C. elegans* Research Community WormBook, doi/10.1895/wormbook.1.100.1, http://www.wormbook.org.

Yochem, J., T. Gu, and M. Han, 1998 A new marker for mosaic analysis in *Caenorhabditis elegans* indicates a fusion between hyp6 and hyp7, two major components of the hypodermis. Genetics 149: 1323–1334.

Yochem, J., S. Tuck, I. Greenwald, and M. Han, 1999 A gp330/megalin-related protein is required in the major epidermis of Caenorhabditis elegans for completion of molting. Development 126: 597–606.

Yochem, J., M. Sundaram, and E. A. Bucher, 2000 Mosaic analysis in *Caenorhabditis elegans*. Methods Mol. Biol. 135: 447–462.

Yochem, J., V. Lazetic, L. Bell, L. Chen, and D. Fay, 2015 *C. elegans* NIMA-related kinases NEKL-2 and NEKL-3 are required for the completion of molting. Dev. Biol. 398: 255–266.

Yu, H., J. K. Mouw, and V. M. Weaver, 2011 Forcing form and function: biomechanical regulation of tumor evolution. Trends Cell Biol. 21: 47–56.

Zalli, D., R. Bayliss, and A. M. Fry, 2012 The Nek8 protein kinase, mutated in the human cystic kidney disease nephronophthisis, is both activated and degraded during ciliogenesis. Hum. Mol. Genet. 21: 1155–1171.

Zannad, F., and A. Radauceanu, 2005 Effect of MR blockade on collagen formation and cardiovascular disease with a specific emphasis on heart failure. Heart Fail. Rev. 10: 71–78.

Zhang, J., W. H. Guo, and Y. L. Wang, 2014 Microtubules stabilize cell polarity by localizing rear signals. Proc. Natl. Acad. Sci. USA 111: 16383–16388.

Zhang, Y., 2008 I-TASSER server for protein 3D structure prediction. BMC Bioinformatics 9: 40.

Zhou, L., Z. Wang, X. Xu, Y. Wan, K. Qu *et al.*, 2016 Nek7 is overexpressed in hepatocellular carcinoma and promotes hepatocellular carcinoma cell proliferation in vitro and in vivo. Oncotarget 7: 18620–18630.

Zugasti, O., J. Rajan, and P. E. Kuwabara, 2005 The function and expansion of the Patched- and Hedgehog-related homologs in *C. elegans*. Genome Res. 15: 1402–1410.

Communicating editor: M. V. Sundaram

Figure S1

A

MLT-2 and ANKS6 alignment

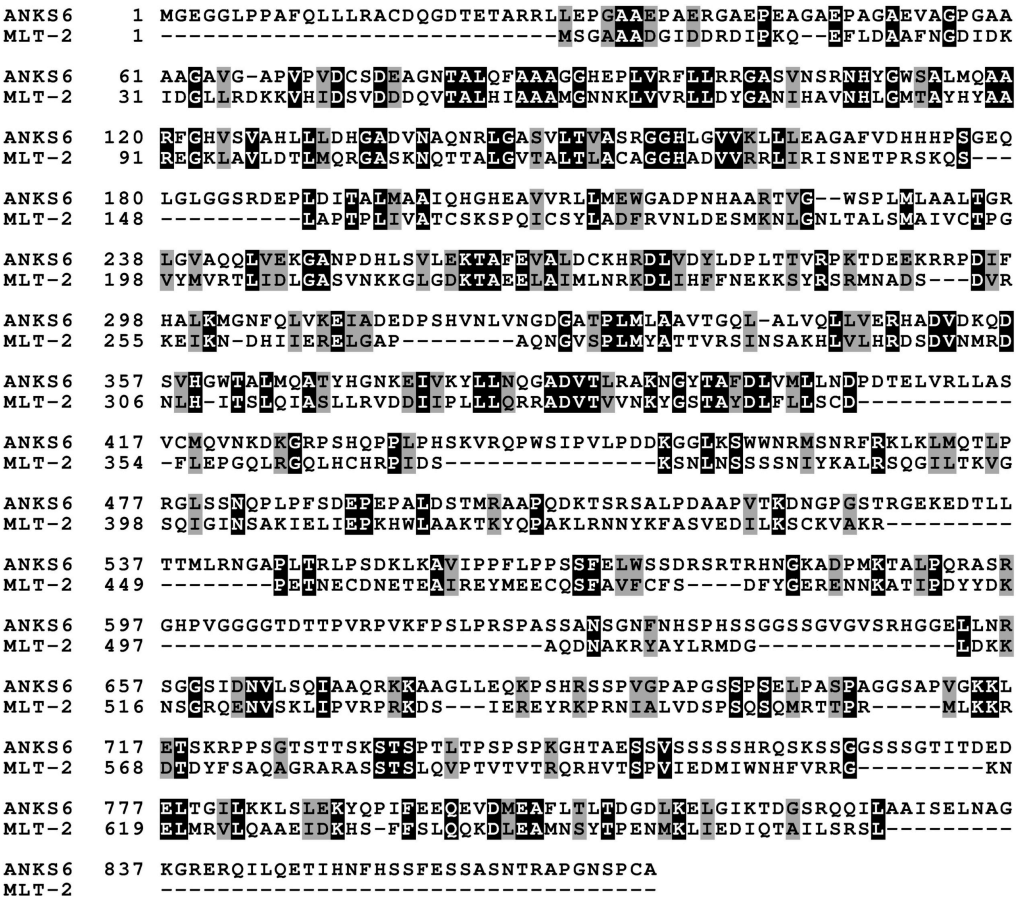

B

MLT-3 and ANKS3 alignment

```
ANKS3     1 -------MSELSDEASEPELLNRSLSMWHGLG---TQVSGEELDVPLDLHTAASIGQYEV
MLT-3     1 MSFRVRFSQERPGVTYVPSSRSGNTDLFNDIFSKPMPIIRNEDHVLMDACTAASIGDENK

ANKS3    51 VKECVQRRELDLNKKNGGGWTPLMYASYIGHDTIVHLLLEAGVSVNVPTPE-GQTPLMLA
MLT-3    61 LKELMKINPNTMIMKNHDGWTPLLYAAYLGHNSVAAFLLDNGAKVDDSTESRWQTPLMMA

ANKS3   110 SSCGNESIAYFLLQQGAELEMKDIQGWTALFHCTSAGHQHMVRFLLDSGANANVREPICG
MLT-3   121 SACGNISVVRLLLGRGANPRLCDKEKRQAIHYASSCCQNVVVDTLLAAGCDPNAAD-SEG

ANKS3   170 FTPLMEAAAAAGHEIIVQYFLNHGVKVDARDHSGATARMLAKQYGHMKIVALMDTYSPSLP
MLT-3   180 TTPVHEAAMAAGHEITFIALLEKGGNLELKNAKGENAAALACDN--NKILQLISEHQAEIA

ANKS3   230 KSLYRSPEKYEDLSSSDESCPAPQRQRPCRKKGVSIHEGPRALARITGIGLGGRAPRPRY
MLT-3   238 K------------------------------------------------------------

ANKS3   290 EQAPPRGYVTFNSSGENPLEEEGLCCRDVTSPINERDVESSSSSSSREEHAFCANLGPVQ
MLT-3   239 ------------------------------------------------------------

ANKS3   350 SSSSSEGLARAQGLSSEASVESNEDSDHACKSSARKQAKSYMKTKNPDSQWPPRAATDRE
MLT-3   239 ------------------------------------------------------------

ANKS3   410 GFLAESSPQTQRAPYSGPQDLAALLEQIGCLKYLQVFEEQDVDLRIFLTLTESDLKEIGI
MLT-3   239 --------QSSKTGNRGPRRLSELLEEMDLSRYIDQFKHENVDLEVFFELKEQDFVDMNI

ANKS3   470 TLFGPKRKMTSAIARWHSSARPPGDALELAYADRLEAEMQELAIQLHKRCEEVEATRGQV
MLT-3   291 A-YGPKKRMLDVIERYKKTGVIRSDAFDAPQGTAMSTKGSSTRESSEKTTATLKSIK---

ANKS3   530 CQEQELRAVVESCLLEQDRAREDLQARLRETWALARDAALVLDQLRACQAELSSRVRQDQ
MLT-3   347 ELNQETKKSVMTALESLGSGQDKVRAQLIS----------ILNNVETISLKVSSHV----

ANKS3   590 PPGAATLGLAVPPADSKGWQASLQAMSLPELSGALEDRVREMGQALCLVTQSLEKLQVLN
MLT-3       ------------------------------------------------------------

ANKS3   650 GKKWRET
MLT-3       -------
```

C

MLT-4 and INVS alignment

```
INVS      1 MNKSENLLFAGSSLASQVHAAAVNGDKGALQRLIVGNSALKDKEDQFGRTPLMYCVLADR
MLT-4     1 MDIRPILYYAAEGSVTELEKEARKLEKQAIKNGSTDVDHFWEILDDKGRNVLFHAAITDN

INVS     61 LDCADALLKAG-----ADVNKTDHSQRTALHLAAQKGNYRFMKLLLT------------R
MLT-4    61 LKNFQFIMKTRRVKKEALLRLTDYNKATVLHWATQYNCKQVVKEIVQTFDKLNPEDLKIL

INVS    104 RANWMQKDLEEMTPLHLTTRHRSPKCLALLLKFMAPGEVDTQ-----DKNKQTALHWSAY
MLT-4   121 HGLILAKDSESVTPLHIAATKQDTKILKIFVEILKTPKVMELFSIVKDKRDRSPLHYAAC

INVS    159 YNNPEHVKLLIKHDSN--------IGIPDVEGKIPLHWAANHKDPSAVHTVRCILDAAPT
MLT-4   181 KVNLEALRILLFVDPNGGPDFGFTVDQRDKFGIIPLMCAVGVNLPQAIPVIRFLEKKKPV

INVS    211 ESLLNWQDYEGRTPLHFAVADGNVTVVDVLTSYESCNITSYDNLFRTPLHWAALLGHAQI
MLT-4   241 SKTR--QNRDGMTALHIAVAARNLEAVQLLIELGSS-VDLVDNEQRTPLHYAAEQGYPEI

INVS    271 VHLLLERNKSGTIPSDSQGATPLHYAAQSNFAETVKVFLKHPSVKDDSDLEGRTSFMWAA
MLT-4   298 VKFLLCNG-ARNSTRDHIGATPAHYAAQFS-VECLKILFAESKITEVNDNEGRSCLMWAV

INVS    331 GKGSDDVLRTMLSLKSDIDINMADKYGGTALHAAALSGHVSTVKLLLENNAQVDATDVMK
MLT-4   356 CAGNIEVINYLIQREDAPKRAACDKNGYTALHLAAMVGHEKVCKILTNQGWSLSERDNHS

INVS    391 HTPLFRACEMGHKDVIQTLIKGGARVDLVDQDGHSLLHWAALGGNADVCQILIENKINPN
MLT-4   416 NTALHLASGRGHTDVLRCLVASGANMNDVDEVGRTAVFWACMGGQAHTLHCMIKELG---

INVS    451 VQDYAGRTPLQCAAYGGYINCMAVLMENNADPNIQDKEGRTALHWSCNNGYLDAIKLLLD
MLT-4   473 ---------FEWRTSG------SVNTRPKCDKNGRTALHAAAVESSACINVLLSIEKEDN

INVS    511 FAAFPNQMENNEERYTPLDYALLGERHEVIQFMLEHGALSIAAIQDIAAFKIQAVYKGYK
MLT-4   518 FLSSPLVGWLDKNGETALHEACLASRIDCILSLLNGGSAVNAFGR----------------

INVS    571 VRKAFRDRKNLLMKHEQLRKDAAAKKREEENKRKEAEQQKGRRSPDSCRPQALPCLPSTQ
MLT-4   563 ------------------------------------------------------------

INVS    631 DVPSRQSRAPSKQPPAGNVAQGPEPRDSRGSPGGSLGGALQKEQHVSSDLQGTNSRRPNE
MLT-4   563 --PQRTPLDCAMQPTVG---------------------------------------APNL

INVS    691 TAREHSKGQSACVHFRPNEGSDGSRHPGVPSVEKSRELRLQIIQRERRRKELFRKKNKAA
MLT-4   582 SVIEYLRSKSALTFAELR-------------------------------------NTAT

INVS    751 AVIQRAWRSYQLRKHLSHLRHMKQLGAGDVDRWRQESTALLLQVWRKELELKFPQTTAVS
MLT-4   604 SVLQRHFKLCKRYKEFILRKK-----------------------------------------

INVS    811 KAPKSPSKGTSGTKSTKHSVLKQIYGCSHEGKIHHPTRSVKASSVLRLNSVSNLQCIHLL
MLT-4       ------------------------------------------------------------

INVS    871 ENSGRSKNFSYNLQSATQPKNKTKP
MLT-4       -------------------------
```

Figure S1. Amino acid sequence alignments. (A–C) CLUSTALW amino acid alignments of *C. elegans* proteins MLT-2 (A), MLT-3 (B), and MLT-4 (C) with their predicted human orthologs ANKS6, ANKS3, and INVS, respectively. Black boxes indicate identical residues; gray boxes, similar residues.

FIGURE S2

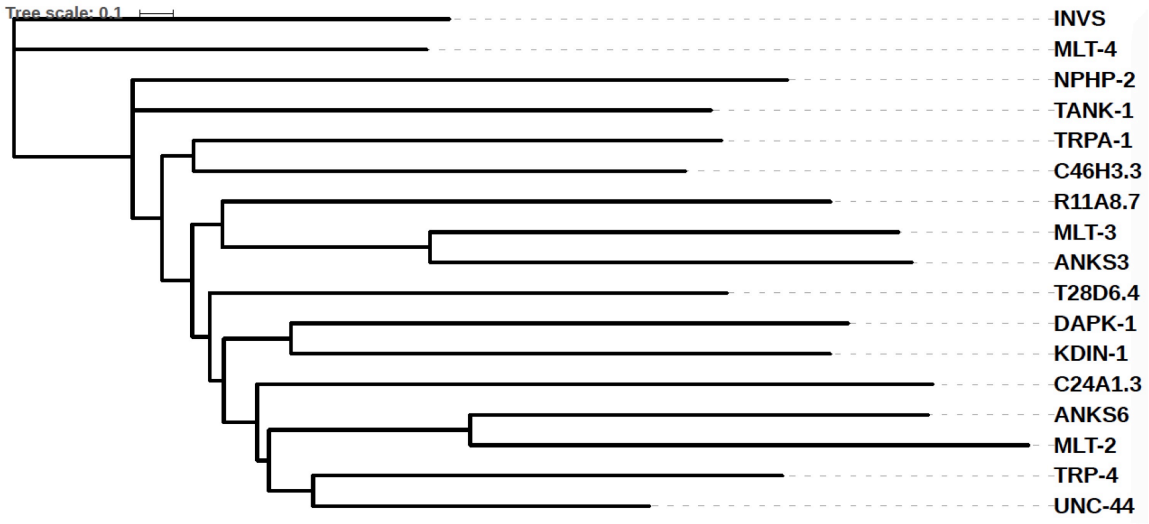

Figure S2. Phylogenetic tree of INVS and its potential orthologs in *C. elegans*. Among the inversin-like proteins examined, MLT-4 is the closest ortholog to INVS in *C. elegans*. Also included are MLT-2, which is closely related to ANKS6, and MLT-3, which is closely related to ANKS3.

FIGURE S3

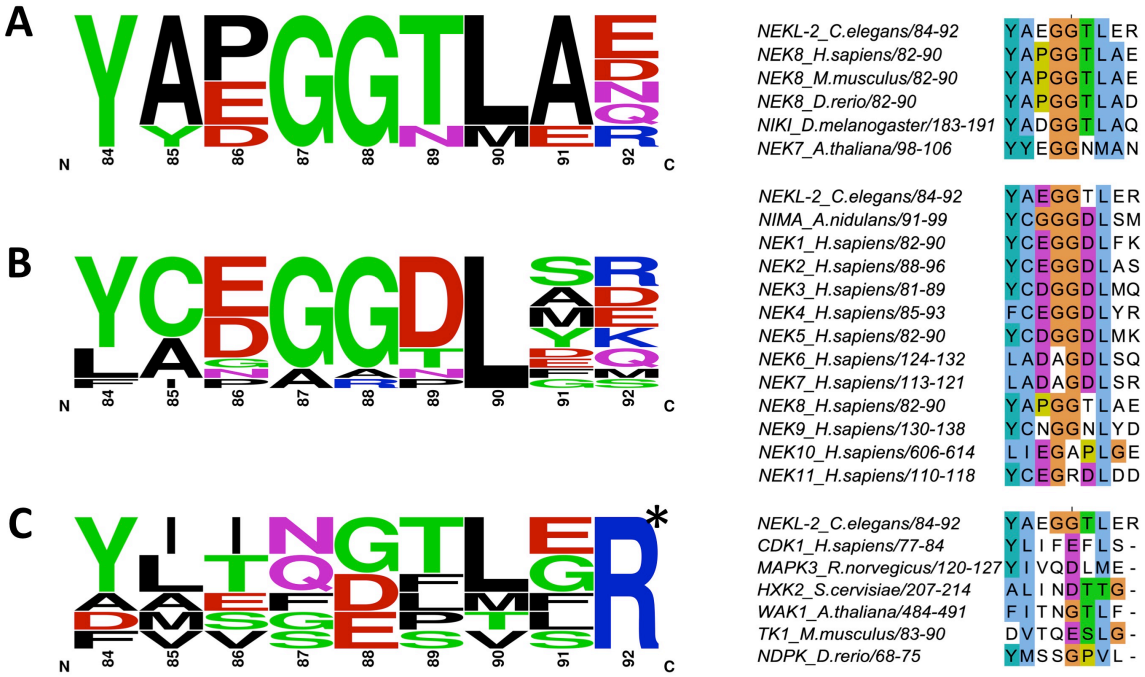

Figure S3. Sequence logos and alignments of the conserved NEKL-2 (aa 84–92) region. (A–C) Frequency plot logos and alignments of the NEKL-2 YAEGGTLER motif in closest orthologs (A), other members of the NIMA kinase family (B), and miscellaneous protein kinases (C). The relative height of the amino acid symbols is proportional to the degree of sequence conservation. Extensive conservation of residues Y84, G87, G88, and L90 was observed across multiple members of the NIMA kinase family. Asterisk in C indicates the R92 residue, which was not aligned to any residue in other proteins.

FIGURE S4

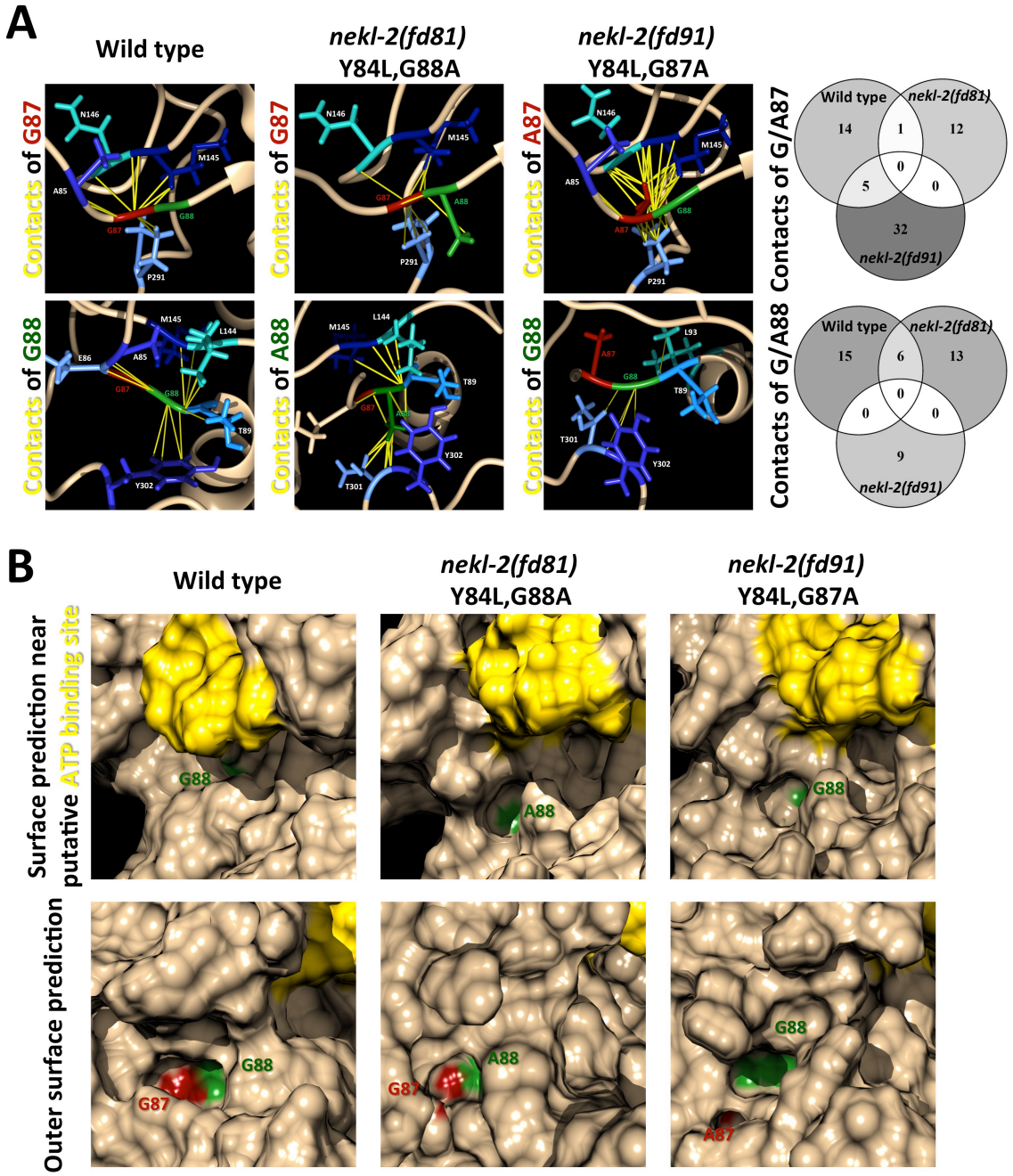

Figure S4. Computational structural comparison of conserved G87 and G88 NEKL-2 residues in wild-type, *fd81*, and *fd91* alleles. (A) Schematic three-dimensional representation of predicted contacts of G/A87 (red, upper panels) and G/A88 (green, lower panels) residues with surrounding amino acids. Interatomic contacts are represented as pseudobonds (yellow). Venn diagrams depict the total number of contacts at aa 87 and 88 along with their conservation in the examined alleles. Note that *fd91* has the greatest number of changes in interatomic contacts at aa 87 and 88. (B) Predicted protein surfaces with annotated G/A87 (red), G/A88 (green), and ATP-binding residues (yellow). Upper panels show changes in surface exposure at aa 88 in mutant alleles *fd81* and *fd91*, close to the predicted ATP-binding residues. Lower panels illustrate exposure of G/A87 and G/A88 residues at the outer protein surface in wild-type, *fd81*, and *fd91* alleles. Residue 87 is more internalized and separated from residue 88 in the *nekl-2(fd91)* allele.

FIGURE S5

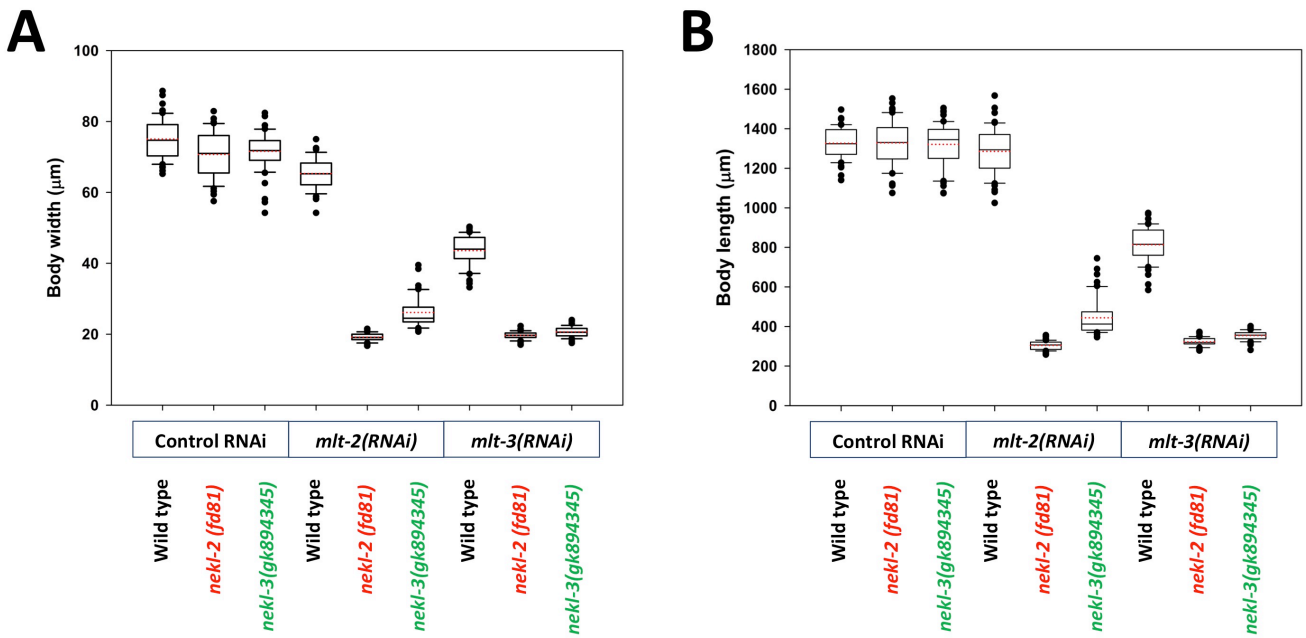

Figure S5. Body measurements in *nekl–mlt* genetic interaction studies. (A, B) Box-and-whisker plots of body width (A) and body length measurements (B). The box includes 50% of data that are closest to the median value (black line). The dotted red line represents mean value for each data set. Outliers that differ by ≥1.5-fold from the lower or upper quartiles are marked with dots. Whiskers span values between the dots and the top or bottom of the boxes. *nekl-2(fd81)* and *nekl-3(gk894345)* alleles were enhanced by *mlt-2(RNAi)* and *mlt-3(RNAi)* treatment. n = 50 for each genotype and treatment.

FIGURE S6

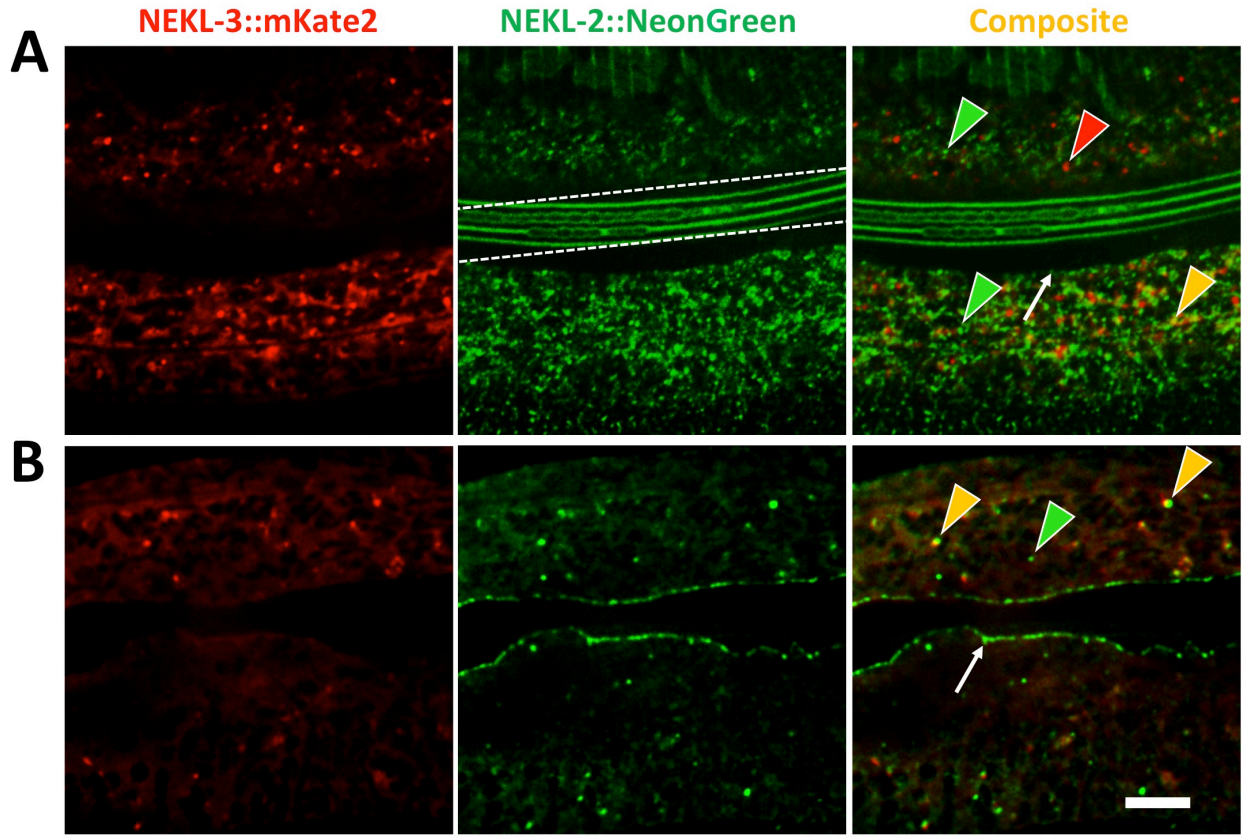

Figure S6. Colocalization of NEKL-2 and NEKL-3. (A,B) Confocal images of colocalization analysis of NEKL-2::NeonGreen and NEKL-3::mKate2. Overlap of the two markers varied between specimens. (A) Adult with little or no significant overlap of NEKL-2 and NEKL-3. White dashed lines demarcate autofluorescent alae. (B) Adult with partial colocalization of NEKL-2 and NEKL-3. Note that NEKL-2 puncta are more abundant in both animals (A,B) and that most or all NEKL-3 puncta also localize to NEKL-2 puncta in B. Red and green arrowheads indicate representative puncta that express only one marker, whereas yellow arrows indicate colocalization. White arrows indicate hyp7–seam cell boundary. Bar = 5 μm.

FIGURE S7

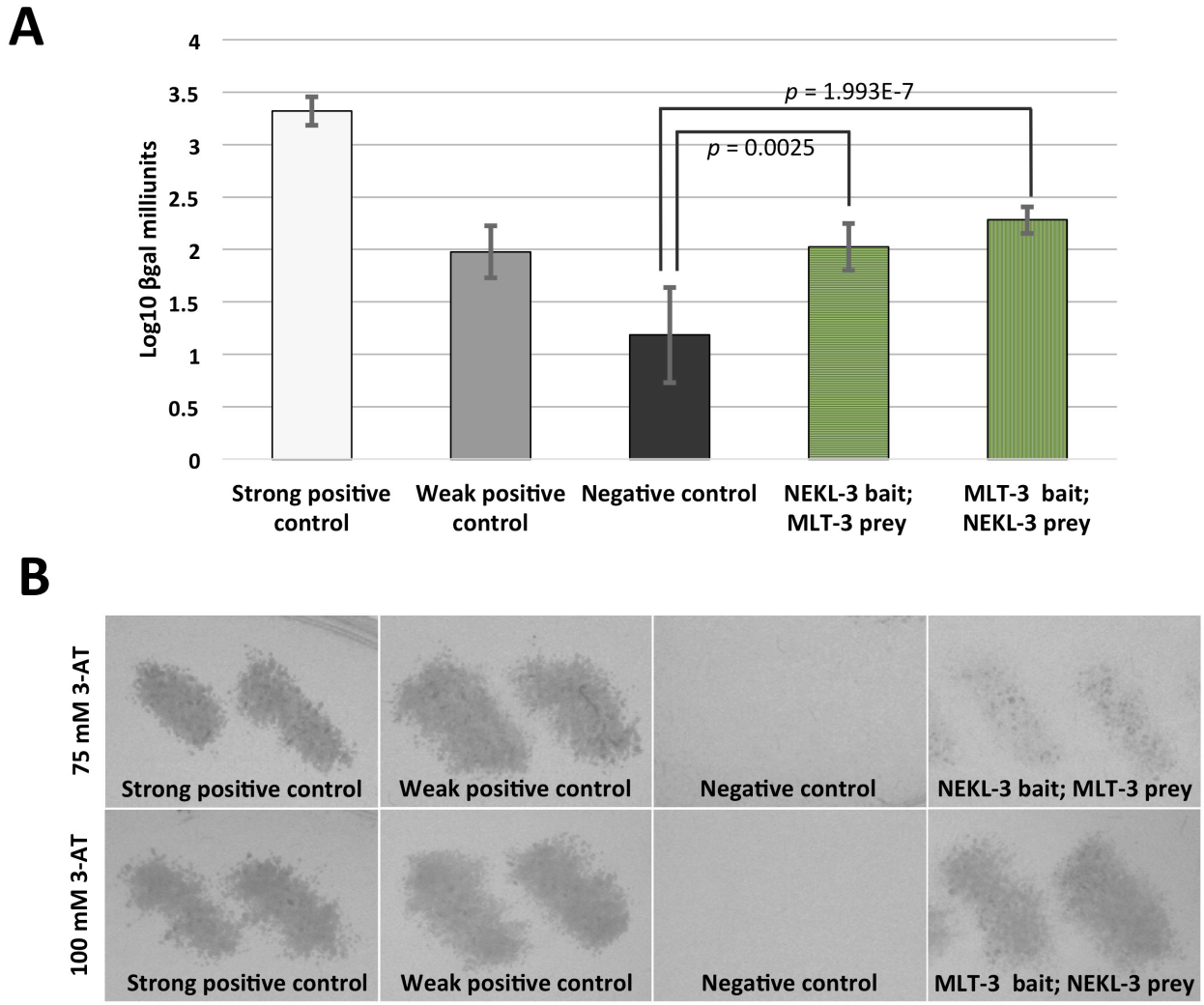

Figure S7. MLT-3 physically interacts with NEKL-3. (A) Yeast two-hybrid analysis revealed a physical interaction between MLT-3 and NEKL-3, which was quantified using β-galactosidase (CPRG) assays. Each value represents the average from 10–12 repeated reactions. Error bars indicate standard deviation; *p*-values, calculated using a Student's *t*-test, are indicated for the relevant comparisons. (B) Growth of the indicated yeast strains on selective SC-Leu-Trp-His + 3-AT medium.

TABLE S1

№	RNAi		Chromosome	Molting defect	
	WormBase ID	Gene name		*lin-35(n745)* background	*rrf-3(pk1426)* background
1	**C01H6.2**	***mlt-2***	**I**	**Yes**	**Yes**
2	K12C11.4	*dapk-1*	I	No	No
3	Y71A12B.4	*trp-4*	I	No	No
4	T28D6.4	-	III	No	No
5	C24A1.3	-	III	No	No
6	**Y39C12A.1**	***mlt-3***	**IV**	**Yes**	**Yes**
7	R11A8.7	-	IV	No	No
8	F36H1.2	*kdin-1*	IV	No	No
9	C29E6.2	*trpa-1*	IV	No	No
10	B0350.2a	*unc-44*	IV	No	No
11	Y32G9A.6	*nphp-2*	V	No	No
12	ZK1005.1	*tank-1*	V	No	No
13	C46H3.3	-	X	No	No

Table S1. RNAi screen of potential Inversin orthologs (other than *mlt-4*) in *C. elegans*. RNAi of *mlt-2*(C01H6.1) and *mlt-3*(Y39C12A.1) were found to cause molting defects in RNAi-sensitized genetic backgrounds.

File S1 MLT-2::mKate2 puncta are dynamic structures. (.zip, 87 KB)

Available for download as a .zip file at
www.genetics.org/lookup/suppl/doi:10.1534/genetics.116.194464/-/DC1/FileS1.zip

File S2 MLT-3::mKate2 dynamics. (.zip, 752 KB)

Available for download as a .zip file at
www.genetics.org/lookup/suppl/doi:10.1534/genetics.116.194464/-/DC1/FileS2.zip

File S3 MLT-4::GFP apical puncta are dynamic structures. (.zip, 752 KB)

Available for download as a .zip file at
www.genetics.org/lookup/suppl/doi:10.1534/genetics.116.194464/-/DC1/FileS3.zip

File S4 MLT-4::GFP puncta interactions. (.zip, 752 KB)

Available for download as a .zip file at
www.genetics.org/lookup/suppl/doi:10.1534/genetics.116.194464/-/DC1/FileS4.zip

MOVIE LEGENDS

Movie 1. MLT-2::mKate2 puncta are dynamic structures. MLT-2::mKate apical puncta exhibit oscillatory and linear motions in hyp7. Note puncta at the top emerging from the boundary with the seam cell into the less densely populated cytosol. Movie speed is 4.7× real time. Bar = 2 μm.

Movie 2. MLT-3::mKate2 dynamics. The MLT-3::mKate2 signal is dispersed throughout the cytosol, although apical puncta are visible, and is very dynamic, displaying circular movements around compartments that do not express the marker. Movie speed is 5× real time. Bar = 2 μm.

Movie 3. MLT-4::GFP apical puncta are dynamic structures. Oscillatory movements of MLT-4 puncta. Movie speed is 5× real time. Bar = 2 μm.

Movie 4. MLT-4::GFP puncta interactions. Apical puncta of MLT-4 sometimes coalesce and/or detach from each other in hyp7. Movie speed is 8.5× real time. Bar = 1 μm.